Bi-allelic *KICS2* mutations impair KICSTOR complex-mediated mTORC1 regulation, causing intellectual disability and epilepsy

Graphical abstract

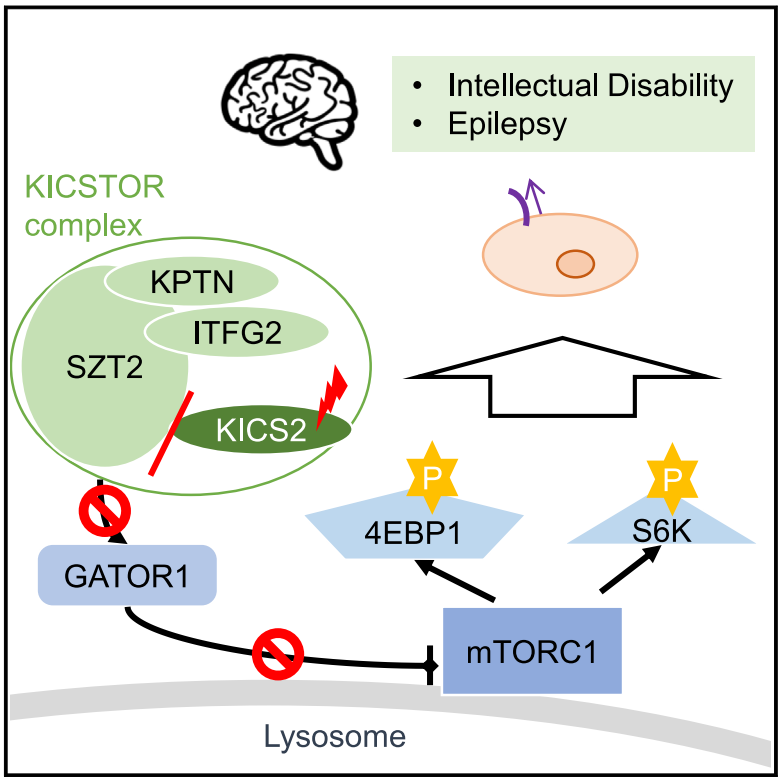

Authors

Rebecca Buchert, Martin D. Burkhalter, Chrisovalantou Huridou, ..., Jonasz J. Weber, Melanie Philipp, Tobias B. Haack

Correspondence

rebecca.buchert@med.uni-tuebingen.de (R.B.), tobias.haack@med.uni-tuebingen.de (T.B.H.)

Sequencing 8 individuals with intellectual disability identified bi-allelic variants in *KICS2*, which encodes a component of the KICSTOR complex. A combination of *in vitro* and *in vivo* analyses demonstrates the physiological relevance of these new variants regarding KICSTOR complex stability, mTORC1 activity, and cilium biology.

Buchert et al., 2025, The American Journal of Human Genetics *112*, 374–393
February 6, 2025
https://doi.org/10.1016/j.ajhg.2024.12.019

CellPress

ARTICLE

Bi-allelic *KICS2* mutations impair KICSTOR complex-mediated mTORC1 regulation, causing intellectual disability and epilepsy

Rebecca Buchert,[1,21,*] Martin D. Burkhalter,[2,21] Chrisovalantou Huridou,[1,3] Linda Sofan,[1] Timo Roser,[4] Kirsten Cremer,[5] Javeria Raza Alvi,[6] Stephanie Efthymiou,[7] Tawfiq Froukh,[8] Sughra Gulieva,[9] Ulviyya Guliyeva,[9] Moath Hamdallah,[10] Muriel Holder-Espinasse,[11] Rauan Kaiyrzhanov,[7] Doreen Klingler,[1] Mahmoud Koko,[12] Lars Matthies,[5,19] Joohyun Park,[1] Marc Sturm,[1] Ana Velic,[13] Stephanie Spranger,[14] Tipu Sultan,[6] Hartmut Engels,[5] Holger Lerche,[12] Henry Houlden,[7] Alistair T. Pagnamenta,[15] Ingo Borggraefe,[4] Yvonne Weber,[12,20] Penelope E. Bonnen,[16] Reza Maroofian,[7] Olaf Riess,[1,17,18] Jonasz J. Weber,[1,3] Melanie Philipp,[2,22] and Tobias B. Haack[1,17,18,22,*]

Summary

Nutrient-dependent mTORC1 regulation upon amino acid deprivation is mediated by the KICSTOR complex, comprising SZT2, KPTN, ITFG2, and KICS2, recruiting GATOR1 to lysosomes. Previously, pathogenic *SZT2* and *KPTN* variants have been associated with autosomal recessive intellectual disability and epileptic encephalopathy. We identified bi-allelic *KICS2* variants in eleven affected individuals presenting with intellectual disability and epilepsy. These variants partly affected KICS2 stability, compromised KICSTOR complex formation, and demonstrated a deleterious impact on nutrient-dependent mTORC1 regulation of 4EBP1 and S6K. Phosphoproteome analyses extended these findings to show that *KICS2* variants changed the mTORC1 proteome, affecting proteins that function in translation, splicing, and ciliogenesis. Depletion of Kics2 in zebrafish resulted in ciliary dysfunction consistent with a role of mTORC1 in cilia biology. These *in vitro* and *in vivo* functional studies confirmed the pathogenicity of identified *KICS2* variants. Our genetic and experimental data provide evidence that variants in KICS2 are a factor involved in intellectual disability due to its dysfunction impacting mTORC1 regulation and cilia biology.

Introduction

Cell growth is controlled through mTORC1 at lysosomes. mTORC1 is activated by the Rag complex, itself regulated by GATOR1 and the KICSTOR complex—composed of KICS2, SZT2, KPTN, and ITFG2—in a nutrient-dependent manner.[1,2] During amino acid deprivation, the KICSTOR complex recruits GATOR1 to the lysosome, inhibiting mTORC1 activity. Consequently, impairment of the KICSTOR complex results in elevated mTORC1 activity, which can be detected on the level of S6K phosphorylation.[1]

Overactivation of the mTORC1 pathway is a recognized cause of several neurodevelopmental disorders, termed mTORopathies, with clinical manifestations including intellectual disability, epilepsy, macrocephaly, and/or overgrowth. Pathogenic variants have been documented in genes of the mTOR pathway, including *TSC1* (MIM: 191100), *TSC2* (MIM: 613254), *PTEN* (MIM: 158350), *MTOR* (MIM: 616638), and in components of the GATOR1 complex (*DEPDC5* [MIM: 620504], *NPRL2* [MIM: 617116], and *NPRL3* [MIM: 617118]).[3–8] Furthermore, bi-allelic pathogenic variants in the KICSTOR complex genes *SZT2* (MIM: 615476) and *KPTN* (MIM: 615637) have been linked to intellectual disability, epilepsy, and macrocephaly,[9,10] while *ITFG2* (MIM: 617421) has been associated with learning disability.[11] To our

[1]Institute of Medical Genetics and Applied Genomics, University of Tübingen, Tübingen, Germany; [2]Department of Experimental and Clinical Pharmacology and Pharmacogenomics, Division of Pharmacogenomics, University of Tübingen, Tübingen, Germany; [3]Department of Human Genetics, Ruhr University Bochum, Bochum, Germany; [4]Division of Pediatric Neurology, Developmental Medicine and Social Pediatrics, Department of Pediatrics, Dr. von Hauner Children's Hospital, Ludwig-Maximilians-University, Munich, Germany; [5]Institute of Human Genetics, School of Medicine & University Hospital Bonn, University of Bonn, Bonn, Germany; [6]Department of Pediatric Neurology, Institute of Child Health, Children's Hospital Lahore, Lahore, Pakistan; [7]Department of Neuromuscular Disorders, UCL Queen Square Institute of Neurology, London WC1N 3BG, UK; [8]Department of Biotechnology and Genetic Engineering, Philadelphia University, Amman, Jordan; [9]MediClub Hospital, Baku, Azerbaijan; [10]Pediatrics Department, An-Najah National University Hospital, Nablus, Palestine; [11]Clinical Genetics Department, Guy's Hospital, Guy's & St Thomas' NHS Foundation Trust, London, UK; [12]Department of Neurology and Epileptology, Hertie-Institute for Clinical Brain Research, University of Tübingen, Tübingen, Germany; [13]Proteome Center Tübingen, University of Tübingen, Tübingen, Germany; [14]MVZ Humangenetik Bremen, Limbach Genetics, Bremen, Germany; [15]NIHR Oxford Biomedical Research Centre, Centre for Human Genetics, University of Oxford, Oxford, UK; [16]Molecular and Human Genetics, Baylor College of Medicine, Houston, TX, USA; [17]Center for Rare Disease, University of Tübingen, Tübingen, Germany; [18]Genomics for Health in Africa (GHA), Africa-Europe Cluster of Research Excellence (CoRE)
[19]Present address: Center of Tropical Medicine, Bernhard Nocht Institute for Tropical Medicine & I. Department of Medicine University Medical Center Hamburg-Eppendorf, Hamburg, Germany
[20]Present address: Department of Epileptology and Neurology, University RWTH Aachen, Aachen, Germany
[21]These authors contributed equally
[22]These authors contributed equally
*Correspondence: rebecca.buchert@med.uni-tuebingen.de (R.B.), tobias.haack@med.uni-tuebingen.de (T.B.H.)
https://doi.org/10.1016/j.ajhg.2024.12.019.

knowledge, no evidence has been reported for a disease association of the last component of the KICSTOR complex, the KICSTOR subunit 2 *KICS2* (MIM: 617420), previously known as *C12orf66*.

Recent studies suggested that the underlying mechanism in individuals carrying *SZT2* variants may be the lack of regulation of mTORC1 activity, as modeling of pathogenic *SZT2* variants in HEK293T cells indicated the hyperphosphorylation of S6K.[12] However, SZT2 interactome studies also revealed possible different functions of the KICSTOR complex.[13] Among the identified interaction partners of SZT2 were several proteins involved in autophagy and ciliogenesis, both being processes modulated by mTOR activity[14,15] and related to neurodevelopment.[16,17] The functional workup of these findings revealed that knocking out SZT2 leads to an increase in the number of ciliated cells and length of cilia. The authors proposed effects on ciliary function as a major pathomechanism in *SZT2*-related disease.

Here, we report on a total of 11 individuals from 8 families with bi-allelic variants in the KICSTOR complex component *KICS2*. We provide evidence that the identified variants disrupt KICSTOR complex formation, compromise mTORC1 regulation, and impact cilia biology. In summary, our clinical and genetic observations in affected individuals, together with the experimental data from cell culture and zebrafish models, provide firm evidence of pathogenic variants in *KICS2* being causative for intellectual disability.

Material and methods

Next-generation sequencing

Informed consent was obtained for all probands prior to sequencing, and studies were conducted in accordance with diagnostic standards and the respective ethics committees of the sequencing institutions. Affected individuals with *KICS2* candidate variants were identified by exome or genome sequencing and data analysis with the respective bioinformatic pipelines of the performing institution as reported previously.[18–26] Matchmaking was facilitated using genematcher and via private communication.[27,28]

Transcriptome sequencing of fibroblasts from individual B:II-4 was conducted using the NEBNext Ultra II Directional RNA mRNA kit as described previously.[29]

All pathogenic variants were reported using reference sequence GenBank: NM_152440.5 (*KICS2*).

Cloning

For transient overexpression in mammalian cell culture, pRK5 plasmid-based cDNA constructs were used, coding for full-length human *KICS2* (pRK5-HA-*C12orf66*; Addgene plasmid #87048; http://n2t.net/addgene:87048; RRID:Addgene 87048), full-length human *SZT2* (pRK5-FLAG-*SZT2*; Addgene plasmid #87034; http://n2t.net/addgene:87034; RRID:Addgene_87034), and full-length human *KPTN* (pRK5-MYC-*KPTN*; Addgene plasmid #87043; http://n2t.net/addgene:87043; RRID:Addgene_87043), all gifts from David Sabatini.[1] We performed mutagenesis on the pRK5-HA-*C12orf66* plasmid using the Phusion Site-Directed Mutagenesis Kit (Thermo Scientific). For pRK5 plasmid transfection into HEK293T (ATCC CRL-3216) cells, Turbofectin 8.0 transfection reagent (OriGene) was used according to manufacturer's instructions.

The zebrafish open reading frame of *kics2* (GenBank: NM_001030090.3) was amplified from a plasmid containing a synthesized *kics2* sequence (Genewiz) using Q5 polymerase (New England Biolabs) and ligated via StuI and XbaI into pCS2+. A truncated version resembling p.K262* in humans was similarly cloned.

Cell treatments for analysis of degradation pathways

To inhibit proteasomal or autophagosomal degradation, HEK293T cells were treated with 0.5 μM epoxomicin (BU-4061T, catalog no. S7038) or 50 nM bafilomycin A1 (Baf-A1; catalog no. S1413) (both Selleckchem) 48 h post-transfection. Dimethyl sulfoxide (DMSO) served as the vehicle control. After a 24-h treatment, the cells were harvested by pelleting at 500 rcf. Proteins were extracted by incubating cell pellets in lysis buffer (10 mM Tris [pH 7.5], 150 mM NaCl, 0.5 mM EDTA, 0.5% [v/v] IGEPAL CA-630) supplemented with cOmplete protease inhibitor cocktail and PhosSTOP phosphatase inhibitor cocktail (both Roche) for 30 min on ice, vortexing every 5 min, and centrifugation at 4°C and 20,000 rcf for 30 min to remove insoluble cell debris. Protein concentrations were measured by Bradford assay using protein assay dye reagent concentrate (Bio-Rad) on a Synergy HT plate reader (BioTek).

coIP and purification of ubiquitinated proteins

Immunoprecipitation (IP) assays were performed as previously described.[30] Briefly, to precipitate tagged or ubiquitinated proteins, 500 μg total protein extracted from transfected HEK293T cells was diluted in 250 μL IP dilution buffer and incubated with 12.5 μL bead slurry of DYKDDDDK Fab-trap agarose (ffa), HA-trap agarose (ata), or ubiquitin-trap agarose (uta) (all Chromotek, Proteintech) for 1 h at 4°C. When necessary, binding control agarose (bab, Proteintech) was used as an IP specificity control. Precipitated proteins were eluted with 2× lithiumdodecylsulphate (LDS) sample buffer and analyzed via western blotting.

Western blot analysis

For SDS-PAGE, 25 μg of total protein, diluted in 1× LDS sample buffer, or samples obtained from IP experiments were heat denatured at 70°C for 10 min and separated on 4%–12% Bolt Bis-Tris Plus gels (Thermo Fisher Scientific). After transfer onto nitrocellulose membranes (Cytiva), total proteins were stained using Ponceau S staining solution or SYPRO Ruby Protein Blot stain (Thermo Fisher Scientific). Membranes were then blocked in 5% (w/v) skim milk powder in 1× TBS for 45 min and incubated with primary and secondary antibodies for immunodetection. For a comprehensive list of primary antibodies used and their dilutions, see Tables S2 and S3. Signals were acquired and quantified using the ODYSSEY FC Imaging System and Image Studio Software 5.2.5 (both LI-COR Biotech).

Generation of gene-edited cell lines

Targeted genome editing for *SZT2* and *KICS2* frameshift variants as well as the c.888C>A (p.Asp296Glu) variant was conducted using the pSpCas9(BB)-2A-GFP (PX458) plasmid (a gift from Feng Zhang [Addgene plasmid #48138; http://n2t.net/addgene:48138; RRID:Addgene_48138][31]) and single-stranded oligodeoxynucleotides (ssODNs). For targeted editing of the *KICS2* c.1178A>G (p.Tyr393Cys) variant, the pCMV_ABEmax_P2A_GFP plasmid (a gift from David Liu [Addgene plasmid #112101;

http://n2t.net/addgene:112101; RRID:Addgene_112101][32]) and the pSPgRNA plasmid (a gift from Charles Gersbach [Addgene plasmid #47108; http://n2t.net/addgene:47108; RRID:Addgene_47108][33]) were used. Sequences of the guide RNAs and ssODNs can be found in Table S4.

HEK293T cells were seeded into 6-well plates and transfected with either pX458 and ssODN repair oligos (5 μL of 10 μM stock) or pCMV_ABEmax_P2A_GFP and pSPgRNA (1.8 μg) using Attractene (Qiagen). 24 h after transfection, the transfected cells expressing GFP were sorted as single cells into 96-well plates using an MA900 cell sorter (Sony Biotechnology). The resulting single cells were then propagated, and gene editing was confirmed with Sanger sequencing. Cell clones with the desired changes were then used in subsequent experiments, and a cell clone that was subjected to the same procedure but found to be wild type was used as the wild-type control.

qPCR of CRISPR-modified HEK293T cells

RNA was extracted from HEK293T cells using an RNeasy kit (Qiagen), and cDNA was obtained using the QuantiTect Reverse Transcription kit (Qiagen). qPCR was performed in triplicates using the QuantiTect SYBR Green PCR kit (Qiagen) on a LightCycler 480 II (Roche Diagnostics). *ACTB*, *PDHB*, and *GAPDH* acted as the endogenous control. Information regarding the primers used will be provided upon request.

Immunoblot analysis of mTORC1 activity

Amino acid starvation was performed as previously described.[1] Briefly, cells were starved for 60 min at 37°C using amino-acid-free DMEM (Genaxxon) supplemented with 10% FBS. Cells were then rinsed with DPBS and directly lysed using Triton lysis buffer supplemented with EDTA-free protease inhibitors (Roche Complete PI EDTA-free; Sigma 11836170001) and PhosSTOP phosphatase inhibitors (Sigma 4906845001) for 20 min. DNA was sheared using the Sonopuls sonicator (Bandelin), and insoluble material was removed by pelleting at 13,000 rcf for 3 min. The protein concentration was measured by Bradford assay using protein assay dye reagent concentrate (Bio-Rad) on a Synergy HT plate reader (BioTek). Proteins were separated on a 10% Bis-Tris gel and transferred to a nitrocellulose membrane (Cytiva). mTORC1 activity was determined using antibodies against S6K and 4EBP1 with GAPDH as the loading control (Table S2). Signals were acquired and quantified using the ODYSSEY FC Imaging System and Image Studio Software 5.2.5 (both LI-COR Biotech). Relative mTORC1 activity values were obtained by first quantifying values using GAPDH as the endogenous control for each sample and experiment, and then relative phosphorylation levels were quantified using the values for 4EBP1 or S6K.

Phosphoproteome nano-LC-MS/MS analysis and data processing

Protein samples were extracted from HEK293T wild-type, KICS2 p.Tyr393Cys, KICS2 p.Asp296Glu, and KICS2 and SZT2 loss-of-function (LOF) cell lines after 1 h amino acid starvation for phosphoproteome analysis with nano-liquid chromatography with tandem mass spectrometry (nano-LC-MS/MS).

Samples were prepared using a protocol for in-solution digest as previously described.[34] For each experiment, different mixes (mix 1: wild type, p.Tyr393Cys, p.Asp296Glu; mix 2: wild type, KICS2 LOF, SZT2 LOF) were prepared in ratio 1:1:1 each with 400 μg, where one part was used for proteome analysis (10 μg).

Dimethyl labeling was performed as described before,[35] followed by label efficiency and label channel mixing checks in separate LC-MS/MS runs. Phosphopeptides were enriched using MagReSyn Ti-IMAC (titanium-immobilized metal affinity chromatography; ReSyn Bioscience) in two consecutive rounds of enrichment using a total amount of 1,200 μg proteins per mix.[34]

All phosphoproteome and proteome samples were analyzed on a Q Exactive HF-X mass spectrometer (Thermo Fisher Scientific). An online-coupled Easy-nLC 1200 UHPLC (Thermo Fisher Scientific) was used to separate peptides on a 20-cm analytical column (75 μm ID PicoTip fused silica emitter [New Objective]) in-house packed with ReproSil-Pur C18-AQ 1.9 μm resin (Dr. Maisch GmbH). Phosphopeptides were eluted using 90 min, and dimethyl-labeled proteome samples were eluted in a 130-min gradient.

Raw files were processed with the MaxQuant software suite (v.1.6.7.0).[36] MS/MS data were searched against the UniProt *Homo sapiens* database (released December 11, 2019; 96,818 entries) containing commonly observed contaminants. The mass tolerance for precursor ions was set to 4.5 ppm and for fragment ions to 20 ppm. All search parameters were kept at default values except for the following: dimethylation for light (28.03 Da), intermediate (32.06 Da), and heavy (36.08 Da) labels was allowed on lysine residues and peptide N termini for phosphoproteome data. For all phospho raw files, phosphorylation of serine, threonine, and tyrosine residues (STY), oxidation of methionine, and protein N-terminal acetylation were set as variable modifications. Carbamidomethylation of cysteine residues was allowed as a fixed modification. All searches were performed in trypsin/P-specific digestion mode.

Data analyses were performed using Perseus software (v.1.6.7.0).[37]

Pathway analysis of phosphoproteome data

Pathway analysis was performed on differentially phosphorylated proteins with a posterior error probability (PEP) < 0.05 using IPA (https://digitalinsights.qiagen.com/IPA).[38] Comparison analysis including a grayscale plot of differentially regulated pathways (Figure 5) was also conducted using IPA. Furthermore, protein function was determined using PubMed. Ciliary proteins were identified using Cildb.[39,40] Venn diagrams were produced using DeepVenn.[41]

Zebrafish maintenance and manipulation

Zebrafish were kept in a circulating water tank system with automatic monitoring and adjustment of pH, conductivity, and temperature (Tecniplast) and fed 4 times a day. The lines used here were wild-type AB and EK lines. Zebrafish husbandry and all experiments described here were approved by local authorities (Veterinary Care Unit at the University of Tübingen and the animal welfare commissioner of the regional board for scientific animal experiments in Tübingen, Germany). Experiments were done in agreement with the European Union Directive 86/609/EEC for the protection of animals used for experimental and other scientific purposes.

Microinjections into fertilized eggs were done at the 1–2 cell stage using a Narishige micromanipulator and a Femtojet microcompressor (Leica) as described before.[42] Loss of Kics2 function was achieved using antisense morpholino oligonucleotides (MOs) designed and synthesized by Gene Tools. For the knockdown of Kics2, the following MOs were used: Kics2 splice-blocking MOs (splMOs; 5′-CAGGTCAACAGGCGGTCTCTCAC-3′) and Kics2 ATG MOs (5′-TGCGGGTCACACATGATAATATGGA-3′). To overexpress different *KICS2* variants, capped RNA was transcribed

from NotI-linearized pCS2+ constructs containing human *KICS2* variants using the mMessage mMachine SP6 kit (Ambion), purified by phenol-chloroform extraction, and dissolved in ultrapure water. To control for manipulation, a standard control MO presumably not targeting any zebrafish gene (Gene Tools) was injected. Clutch quality was assessed based on non-injected embryos from the same breeding tank and day. After injection, embryos were raised to the desired stages by incubation at 28.5°C. Rapamycin (LC Laboratories) treatment was done from the tail-bud stage on by adding 500 nM of the compound directly to the embryo water. DMSO was used as a vehicle control.

Fibroblast cell culture and nucleofection

Immortalized forearm skin fibroblasts (1BR3, Sussex Cell Culture Collection) were cultured in MEMα supplemented with 10% heat-inactivated fetal calf serum (FCS) and 1% penicillin/streptomycin (all from Gibco) at 37°C in an incubator with 5% CO_2. Nucleofection was done essentially as described before[43] using Dharmacon's Smartpool small interfering RNAs (siRNAs) against *KICS2* or a non-targeting pool, the Amaxa Cell Line Nucleofector Kit R, program U-023, and an Amaxa nucleofector II (both Lonza). After nucleofection, cells were seeded directly onto glass cover slips for subsequent immunofluorescence or into 6-well plates for RNA isolation. After 48 h of culture, cells were changed to starvation medium containing only 0.1% FCS. All analyses were performed after 3 days of starvation.

The cell line has been authenticated and regularly tested for mycoplasma contamination.

Immunofluorescence

Embryos were fixed in 4% buffered paraformaldehyde, washed several times using PBS, incubated in distilled water for 5 min, and permeabilized in ice-cold acetone for 5 min at −20°C. After another round of incubation in water, embryos were rinsed several times using PBS containing 0.1% Tween 20 (PBST) and blocked at least for 1 h in 10% normal goat serum diluted in PBST containing 1% DMSO (PBDT). Antibodies were diluted in blocking buffer and incubated overnight at 4°C (primary antibodies) and for several hours at room temperature in the case of secondary antibodies. Before imaging, embryos or parts thereof were embedded in Vectashield containing DAPI (Vectorlabs) between two coverslips.

Nucleofected fibroblasts were fixed in ice-cold methanol, washed twice using PBS, and permeabilized for 15 min using 0.1% Triton X-100 in PBS. After blocking using 10% FCS, cover slips were incubated with primary antibodies at 4°C overnight, washed three times with PBS, and probed with secondary antibodies for 1–2 h at room temperature. After three more washes with PBS, cover slips were mounted onto slides using Vectashield containing DAPI.

The antibodies used were as follows: mouse anti-acetylated tubulin (1:500, Sigma, cat. no. T6793), rabbit anti-γ-tubulin (1:500, Sigma, cat. no. T5192), rabbit anti-PKCζ (1:500, Santa Cruz Biotechnology, cat. no. sc-216), and rabbit anti-phospho-S6 (1:500, Cell Signaling, cat. no. 5364S). Alexa Fluor-coupled secondary antibodies were used to detect primary antibodies: donkey anti-mouse immunoglobulin (Ig)G (H+L) Alexa Fluor 568 (Invitrogen, cat. no. A10037, 1:1,000) and goat anti-rabbit Alexa 488 (Invitrogen, cat. no. A11008, 1:1,000).

qPCR analysis of nucleofected cells

After 3 days of serum starvation, cells were directly lysed in the wells in order to isolate total RNA using Zymo's Quick-RNA Miniprep kit (including DNase I digest of remaining genomic DNA). cDNA of equal amounts of RNA was generated using the Protoscript II Kit (New England Biolabs). qPCR was done in triplicates with Luna Universal probe qPCR Master Mix (New England Biolabs) and the Roche Universal Probe System on a QuantStudio 3 thermal cycler (Applied Biosystems). *SDHA* was used for internal reference as a housekeeping gene. Information regarding the primers and probes used is readily available upon request.

Test for splice blocking

Total RNA was isolated of 24 h post-fertilization (hpf) zebrafish embryos using the Quick-RNA Miniprep kit and digested using DNase I (Zymo Research). Equal amounts of RNA were reversely transcribed into cDNA using the Protoscript II Kit (New England Biolabs), before a PCR was done using primers spanning the entire intron between exons 2 and 3 (forward: 5′-TGG TCA GTC GTT CTT CAG CC-3′, reverse: 5′-GGG TTT GGA GTT CCT CAG GG-3′). Only in properly spliced transcripts could a band of 1,075 bp be obtained. As a housekeeping reference, a 319-bp fragment of *gapdh* was amplified (forward: 5′-CCA TCA ACG GTC TTC TGT GTT-3′, reverse: 5′-ACA TTA AGT GGG GTG ATG CAG-3′).

In situ hybridization

Embryos were fixed at the desired stages using 4% buffered paraformaldehyde and processed using standard protocols of *in situ* hybridization. DIG-labeled probes for *southpaw* (*spaw*), *cardiac myosin light chain 2* (*cmlc2*), and *insulin* (*ins*) have been described before.[44] In order to generate an antisense probe against zebrafish *kics2* (GenBank: NM_001030090.3), a 1,075-bp fragment was amplified from cDNA of 24 hpf zebrafish embryos using the Expand long template polymerase (Roche) and cloned by TOPO TA cloning (Invitrogen) into pCRII. After linearization with XbaI, an antisense probe was transcribed using SP6 RNA polymerase (New England Biolabs) and DIG labeling mix (Roche). The same plasmid was linearized using SpeI and transcribed with T7 RNA polymerase (New England Biolabs) to synthesize a sense probe.

Imaging

Live embryos and embryos processed by *in situ* hybridization were imaged with a Leica M125 stereo microscope and an IC80HD color camera. Cilia and phospho-S6 immunofluorescence were imaged on a Leica Stellaris 5 confocal platform equipped with a white light laser and the LASX software. Cilia length was measured with the help of the FIJI Neurite Tracer plugin.[45]

Statistics

All statistical analyses were done with GraphPad's Prism v.9. All data were first analyzed for normal distribution with Prism's Shapiro-Wilk test before a parametric or non-parametric test was applied. An alpha value smaller than 0.05 was considered significant.

Results

Identification of *KICS2* variants in individuals with intellectual disability

Exome or genome sequencing and subsequent matchmaking led us to identify a total of 11 affected individuals from 8 families with bi-allelic variants in *KICS2*

(GenBank: NM_152440.5; Table 1; Figures 1 and S1; supplemental note). All affected individuals had mild to moderate intellectual disability, and 8 individuals presented with seizures, sometimes only febrile. Seizure type and onset varied among the study population, but they mostly responded well to medication. While intellectual disability and seizures were the most commonly occurring clinical features across these 11 individuals, some additional features were noted in a subset of affected individuals. Three individuals had varying degrees of hearing impairment. Body measurements were within the normal range, with the exception of two individuals who presented with (relative) macrocephaly. Generally speaking, body length was in the lower normal range, while head circumference was in the higher normal range. Facial dysmorphism was assessed in 6 of the affected individuals, all of whom were noted to have some abnormalities, including a short, deep philtrum, broad nose, and prominent forehead.

Across these 8 families, a total of 7 different disease alleles were identified, all of which exhibited recessive inheritance (Table S1). These pathogenic *KICS2* variants included two highly conserved missense variants (c.1178A>G [GenBank: NM_152440.5]; p.Tyr393Cys and c.888C>A [GenBank: NM_152440.5]; p.Asp296Glu), four predicted nonsense variants (c.7G>T [GenBank: NM_152440.5]; p.Glu3*, c.236-2delA [GenBank: NM_152440.5]; p.Gly79Valfs*18, c.780del [GenBank: NM_152440.5]; p.Lys260Asnfs*18, and c.784A>T [GenBank: NM_152440.5]; p.Lys262*), and a deletion of 1.1 Mb that spanned *KICS2*. Consanguinity was noted in most families in this study, and consequently, most affected individuals were homozygous for a pathogenic variant; only one family was compound heterozygous for two pathogenic variants. The variants that appeared most often in this cohort were c.236-2delA (GenBank: NM_152440.5; p.Gly79Valfs*18) (families B and C) and c.1178A>G (GenBank: NM_152440.5; p.Tyr393Cys) (families G and H).

All variants segregated with the disease and were exceedingly rare or absent from gnomAD v.3.1.[46] For the splice variant c.236-2delA, we conducted whole-transcriptome sequencing on mRNA from fibroblasts of individual B:II-4. This experiment demonstrated that this variant resulted in a deletion of the first 8 bp of exon 2, consistent with the SpliceAI prediction (Table S1), and predicted a frameshift and premature stop codon p.Gly79Valfs*18.

KICS2 frameshift variant triggers enhanced degradation via the UPS

To investigate whether the detected variants influence the protein levels of both KICS2 and other components of the KICSTOR complex, we overexpressed wild-type HA-KICS2, as well as missense variants p.Tyr393Cys and p.Asp296Glu, and the truncating variant p.Lys260Asnfs*18 in HEK293T cells, together with SZT2 and KPTN. Western blot analysis demonstrated comparable protein levels of wild-type KICS2 and its missense variants, whereas levels of the p.Lys260Asnfs*18 variant, which migrated at a lower molecular weight, as expected, were reduced by approximately 70% (Figures 2A and 2B). Interestingly, additional bands migrating above KICS2 p.Lys260Asnfs*18 were observed, indicating a potential post-translational modification of the truncated variant (Figure 2A). Aside from a weak but significant reduction of SZT2 levels in the presence of KICS2 p.Tyr393Cys, SZT2 and KPTN levels remained largely unchanged upon variant co-expression (Figure 2B).

As the additional high-molecular-weight bands observed for KICS2 p.Lys260Asnfs*18 might represent ubiquitinated forms of the truncated protein, targeting it for a proteolytic degradation, we performed IP experiments with HEK293T cells overexpressing wild-type KICS2 and the p.Lys260Asnfs*18 variant to purify their ubiquitinated forms. Western blot-based analysis of the ubiquitination-specific IP demonstrated that both wild-type KICS2 and KICS2 p.Lys260Asnfs*18 are ubiquitinated, and the bands observed above the truncated variant correspond to this detected ubiquitination pattern (Figures 2C–2E).

To determine which major proteolytic pathway is responsible for the degradation of KICS2 and its truncated variant, we overexpressed both versions in HEK293T cells for 72 h and inhibited proteasomal degradation or autophagy by administering the pharmacological inhibitor epoxomicin or Baf-A1, respectively (Figures 2F and 2G). After confirming the successful inhibition of both pathways by detecting the accumulation of the respective markers, K48-linked polyubiquitin and LC3B-II, we analyzed the changes in KICS2 levels (Figure 2F). While autophagy inhibition did not affect the levels of wild-type KICS2, KICS2 p.Lys260Asnfs*18, or their ubiquitinated protein species, proteasomal inhibition led to a significant increase in the unmodified and ubiquitinated forms of both proteins. Importantly, quantification demonstrated significantly higher baseline ubiquitination of KICS2 p.Lys260Asnfs*18 compared to the wild-type form, indicating enhanced targeting of the truncated variant for degradation via the ubiquitin-proteasomal system (UPS) (Figure 2G). These results establish KICS2 as a substrate of the UPS and demonstrate that truncating variants, such as p.Lys260Asnfs*18, lead to enhanced degradation and subsequent loss of the protein.

KICS2 variants disturb interaction with components of the KICSTOR complex

Both missense and truncating variants of KICS2 may affect the interaction with other key components of the KICSTOR complex. To investigate this, we performed coIP assays of HEK293T cells co-expressing SZT2, KPTN, and either wild-type KICS2 or its p.Tyr393Cys, p.Asp296Glu, and p.Lys260Asnfs*18 variants. The interactions were analyzed by western blotting. When immunoprecipitating SZT2 (Figures 3A–3C), which serves as a linker between the other components of the KICSTOR complex,[1] no major changes in the KPTN interaction were observed in the presence of KICS2 variants. However, the interaction of SZT2 with the KICS2 variants was significantly reduced, with p.Tyr393Cys, p.Asp296Glu, and

Table 1. Phenotypes of affected individuals

Family	A	B	B	C	C	D	E	F	G	G	H
Individual	A:II-1	B:II-2	B:II-4	C:II-1	C:II-3	D:II-3	E:II-1	F:II-1	G:II-2	G:II-3	H:II-1
Consanguinity	parents 1° cousins	parents 1° cousins	parents 1° cousins	parents 1° cousins	parents 1° cousins	parents 1° cousins	no	parents are cousins	N/A	N/A	parents are cousins
Variant	c.7G>T (p.Glu3*)	c.236-2delA (p.Gly79Valfs*18)	c.236-2delA (p.Gly79Valfs*18)	c.236-2delA (p.Gly79Valfs*18)	c.236-2delA (p.Gly79Valfs*18)	c.780del (p.Lys260Asnfs*18)	c.784A>T (p.Lys262*)/1.1 Mb deletion	c.888C>A (p.Asp296Glu)	c.1178A>G (p.Tyr393Cys)	c.1178A>G (p.Tyr393Cys)	c.1178A>G (p.Tyr393Cys)
Zygosity	hom	hom	hom	hom	hom	hom	comp het	hom	hom	hom	hom
Sex	m	m	m	f	m	m	f	m	m	m	f
Age at last examination	15 y	16 y	10 y	16 y, 10 mo	7 y, 7 mo	7 y	4 y	10 y	19 y	17 y	12 y
Birth weight, g (SD)	3,200 (−1.25)	1,400 (−4.69)	2,500 (−2.38)	1,320 (P44; −0.15)	normal	2,600 (−2.23)	2,236 (−2.39)	N/A	N/A	N/A	2,390 (−2.34)
Birth length, cm (SD)	51 (−0.66)	N/A	N/A	41 (+0.38)	normal	N/A	N/A	N/A	N/A	N/A	45 (−2.62)
Birth OFC, cm (SD)	N/A	N/A	N/A	28 (0)	N/A	N/A	N/A	N/A	N/A	N/A	32 (−2.50)
Height, cm (SD)	183 (+1.77)	168 (−0.44)	128 (−1.64)	at 13 years, 147 (−1.94)	N/A	N/A	97 (−0.89)	N/A	N/A	N/A	144 (−1.61)
Weight, kg (SD)	81 (+1.75)	N/A	N/A	at 13 years, 31.8 (−2.77)	N/A	35 (+2.42)	13.8 (−1.71)	N/A	N/A	N/A	37 (−1.04)
OFC, cm (SD)	63 (+5.4)	54 (−0.74)	54 (+0.84)	at 13 years, 55 (+0.68)	N/A	N/A	52 (+1.56)	relative macrocephaly	N/A	N/A	55.3 (+1.24)
Walking (age)	1 y, 5 mo	2 y	2 y	walking with assistance at the age of 16 y	1 year, 11 mo	3 y	24 mo	N/A	N/A	N/A	18 mo
Speech abilities	normal	delay	no speech	no speech	babbling	8–10 words	delay	verbal dyspraxia	N/A	N/A	simple combination of words
Comprehension	normal	delay	very limited	N/A	N/A	N/A	delay	N/A	N/A	N/A	very limited
Regression (age)	no	no	no	N/A	N/A	yes	no	N/A	N/A	N/A	no
Intellectual disability	mild	moderate	severe	severe	yes	moderate	moderate	yes	yes	yes	moderate
Seizure onset (type)	at 6 mo (cyanotic autonomic focal seizures and rare tonic-clonic)	yes	yes	at 6 mo (not specified)	no	yes (focal mainly, sometimes bilateral tonic clonic and rarely myoclonic jerks)	febrile	yes (tonic posturing and myoclonic jerks)	no	no	6 y (generalized tonic-clonic)

(*Continued on next page*)

Table 1. ***Continued***

Family	A	B	B	C	C	D	E	F	G	G	H
Antiepileptic treatment	valproate and carbamazepine in infancy, taking levetiracetam now	carbamazepine + valproate	carbamazepine + valproate	yes (no information)	no	N/A	N/A	N/A	no	no	valproate
Response to treatment	partial response to levetiracetam	seizure-free under medication	seizure-free under medication	improvement after treatment for 6 mo	–	N/A	N/A	N/A	–	–	yes, epilepsy well controlled
MRI anomalies	no	not performed	not performed	unspecific gliosis in right frontal semioval center	not performed	few T2W hyperintensities in the periventricular white matter predominantly in the parieto-occipital regions	non-specific white matter gliosis in the parietal and frontal regions	N/A	N/A	N/A	no
Hypotonia	yes	N/A	N/A	N/A	N/A	yes	yes	no	N/A	N/A	yes
Hypertonia	no	N/A	N/A	N/A	N/A	no	no	no	N/A	N/A	no
Movement disorders	no	N/A	N/A	hand washing movements	N/A	yes	no	no	dystonia	dystonia	no
Stereotypies	no	N/A	N/A	repetitive head circling, fingernail biting	N/A	N/A	N/A	N/A	N/A	N/A	yes
Behavioral anomalies	no	N/A	N/A	laughing fits	N/A	autism, ADHD, aggression	N/A	self-destructive behaviors	N/A	N/A	ADHD
Sleeping	normal	normal	normal	difficulty sleeping through the night	difficulties to fall asleep	N/A	N/A	N/A	N/A	N/A	impaired
Facial dysmorphism	hypertelorism	short, deep philtrum	short, deep philtrum	discrete synophrys; short, broad nose with broad nasal bridge; low-hanging columella; short, deep philtrum; high and narrow palate	broad nose with broad nasal bridge, rather deep philtrum, low-hanging columella	N/A	N/A	N/A	N/A	N/A	short nose with anteverted nares, prominent forehead with depressed nasal bridge
Hearing	normal	mild bilateral hearing impairment	normal	N/A	N/A	normal	normal	normal	conductive hearing impairment	conductive hearing impairment	normal

(*Continued on next page*)

Table 1. ***Continued***

Family	A	B	B	C	C	D	E	F	G	G	H
Vision	normal	normal	normal	strabismus convergens	N/A	normal	normal	normal	N/A	N/A	hyperopia
Other anomalies	cannot run, sialorrhea, fast fatiguability	hemophilia type VIII, simple incomplete syndactyly	aortic stenosis (2.5 y)	hypopigmented maculae covering entire integument, Langerhans cell histiocytosis as newborn; episodes of near-daily vomiting	perinatal asphyxia	N/A	none	N/A	N/A	N/A	clinodactyly 5th fingers bilaterally
Further, previous testing	no	FraX, karyotyping unremarkable	no	karyotyping, CMA, subtelomere screening, UBE3A-MLPA, FraX, MECP2 gene sequencing and MLPA unremarkable	karyotyping, CMA, FraX unremarkable	N/A	N/A	N/A	N/A	N/A	array-CGH, karyotyping unremarkable
Other WES result	no	no	no	het VUS in *AVIL*	het VUS in *AVIL*	no	no	no	no	no	het VUS in *CNTNAP2*

OFC, occipitofrontal circumference; f, female; m, male; y, years; mo, months; N/A, not available; het; heterozygous; hom, homozygous; comp het., compound heterozygous; VUS, variant of unknown significance; WES, whole-exosome sequencing; ADHD, attention-deficient hyperactive disorder; CMA, chromosomal microarray analysis; MLPA, multiplex ligation-dependent probe amplification; CGH, comparative genomic hybridisation.

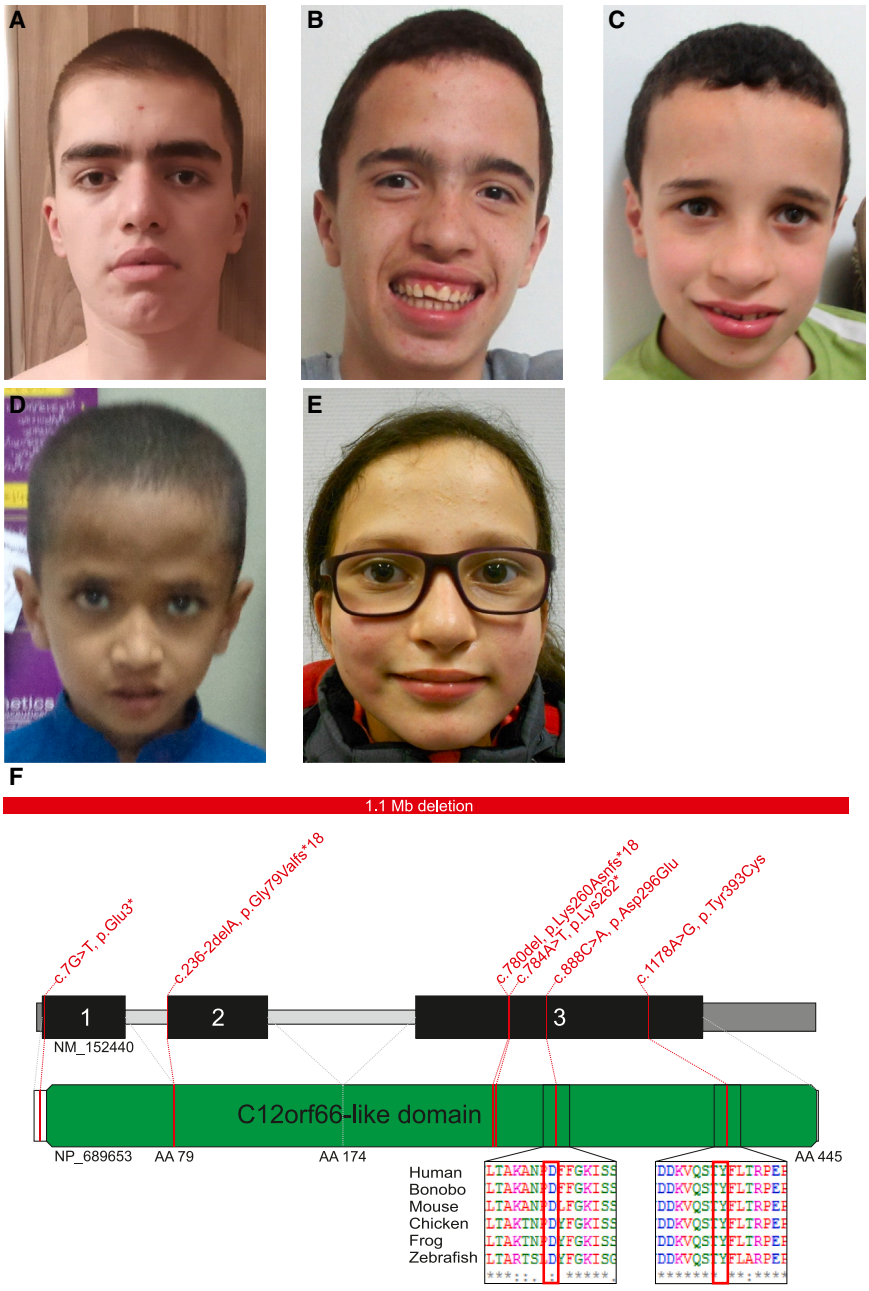

Figure 1. Pictures of individuals with *KICS2* variants and the positions of the variants within the gene

(A–E) Affected individuals show a short, deep philtrum, a short, broad nose, a broad nasal bridge, and a prominent forehead: (A) individual A:II-1 at age 15 years, (B) individual B:II-2 at age 16 years, (C) individual B:II-4 at age 10 years, (D) individual D:II-3 at age 7 years, and (E) individual H:II-1 at age 12 years.

(F) *KICS2* gene structure with the identified variants; identified missense variants are localized in highly conserved regions.

p.Lys260Asnfs*18 showing reductions of approximately 34%, 14%, and 67%, respectively (Figure 3C). Notably, a previously reported potential interaction partner of SZT2, LAMP2,[47] was not detected in our coIP.

To confirm our results, we repeated our experiments by immunoprecipitating KICS2 and analyzing the co-precipitated interaction partners (Figures 3D–3F). In this approach, both SZT2 and KPTN exhibited reduced binding, showing comparable trends. Importantly, while the p.Tyr393Cys variant presented a stronger reduction in interaction with SZT2 and KPTN than KICS2 p.Asp296Glu, the C-terminally truncated p.Lys260Asnfs*18 variant showed no co-precipitation of SZT2, highlighting that the C terminus of KICS2 is essential for SZT2 binding (Figures 3E and 3F). Moreover, the stronger effect of the p.Tyr393Cys variant narrows down the interaction site to a region around the respective amino acid. Interestingly, KPTN interaction was not abolished in the absence of the KICS2 C terminus, suggesting that KICS2 may also bind directly to KPTN through its remaining sequence.

To confirm this, we repeated the coIP experiments with wild-type KICS2 in the presence or absence of SZT2. As suggested by the previous coIP results, the lack of SZT2 overexpression led only to a modest reduction in KPTN binding, with KICS2 still able to bind KPTN efficiently (Figures S2A and S2B). These results show that missense variants in *KICS2* may interfere with the formation of the KICSTOR complex, with the C terminus of KICS2 being crucial for SZT2 binding, while the N terminus likely mediates a direct interaction with KPTN.

Cell-based modeling of *KICS2* variants indicates disturbed mTORC1 regulation

Since *KICS2* variants showed negative effects on the interaction of KICSTOR components in our coIP experiments, we examined whether these perturbations could have functional repercussions on mTORC1 activity downstream of the KICSTOR complex. For this, we modeled both identified *KICS2* missense variants as well as a LOF variant by introducing a frameshift in exon 3 in HEK293T cells using the CRISPR-Cas9 system. When testing for *KICS2* expression using qPCR, we found that cells harboring a frameshift in exon 3 have reduced *KICS2* expression; nevertheless, a significant amount of *KICS2* mRNA escapes nonsense-mediated mRNA decay (Figure S3). However, since our previous experiments with expression constructs of *KICS2* truncating variants showed a significant protein instability and negligible interaction with

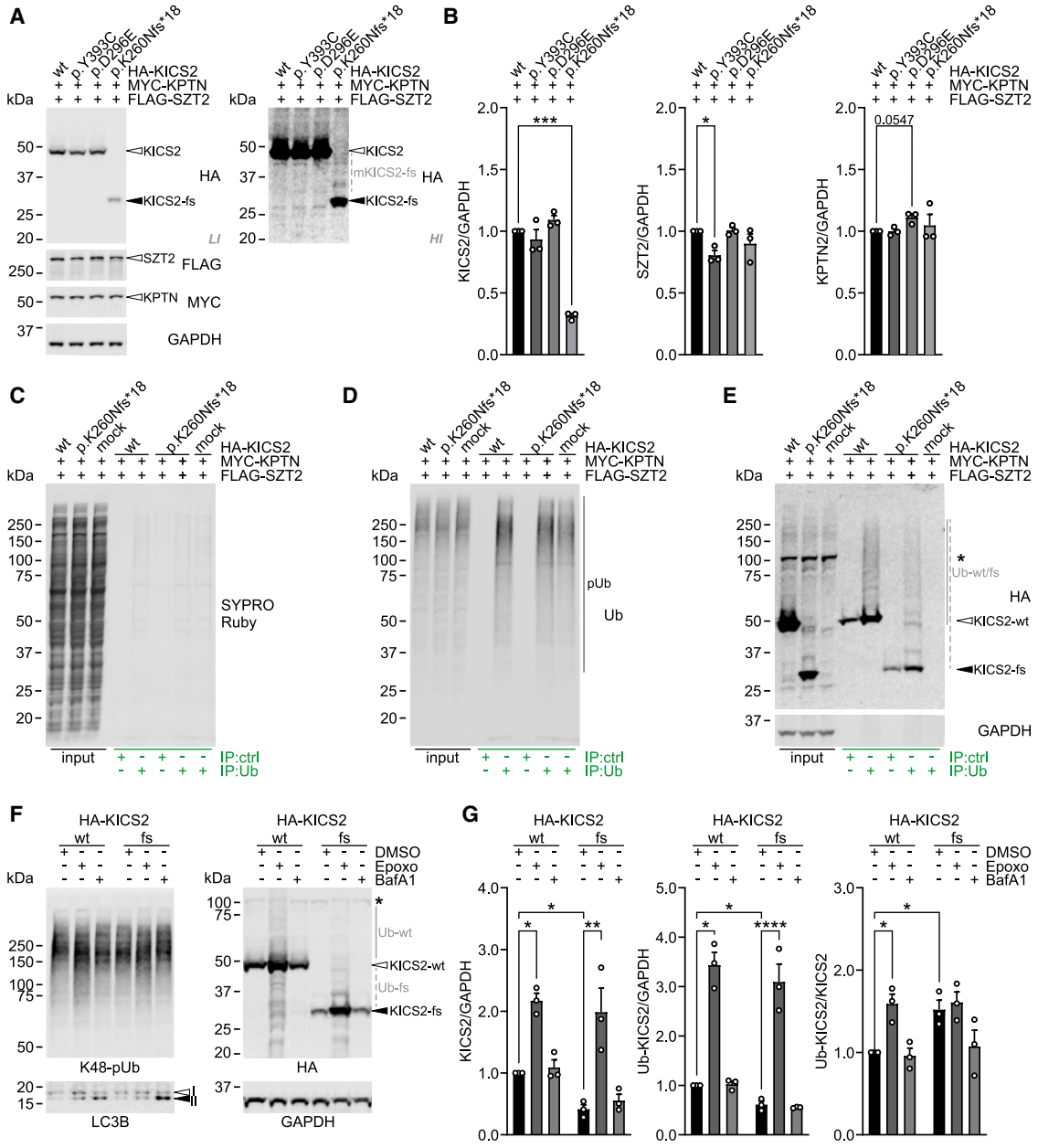

Figure 2. Missense variants do not alter KICS2 levels or influence KICSTOR components, but the p.Lys260Asnfs*18 variant is ubiquitinated and rapidly degraded by the UPS system

(A) Western blot analysis of HEK293T cells overexpressing wild-type (WT) HA-tagged KICS2 or its variants, along with KICSTOR components FLAG-tagged SZT2 and MYC-tagged KPTN, shows a strong reduction in levels of the C-terminally truncated variant p.Lys260Asnfs*18, while missense variants p.Tyr393Cys and p.Asp296Glu do not affect KICS2 amounts. High-intensity display reveals multiple high-molecular-weight, potentially post-translationally modified forms of KICS2 p.Lys260Asnfs*18 (KICS2-fs [frameshift], marked with a dashed gray line). Overexpressed proteins were detected using tag-specific antibodies. GAPDH served as the loading control. *LI*, low intensity; *HI*, high intensity.

(B) Relative quantification of HA-KICS2, FLAG-SZT2, and MYC-KPTN from $n = 3$ biological replicates (***$p < 0.001$ and *$p < 0.05$, one-sample t test and two-way ANOVA followed by Tukey's multiple comparison test).

(C–E) Analysis of putatively ubiquitinated (Ub) forms of KICS2 using Ub-Trap immunoprecipitation (IP) of lysates obtained from HEK293T cells transfected with HA-tagged WT KICS2 or KICS2 p.Lys260Asnfs*18 (KICS2-fs), or an empty control vector (mock), along with MYC-tagged KPTN and FLAG-tagged SZT2. Control beads (ctrl) were used for confirming specificity. Western blot of input samples and eluates, followed by SYPRO Ruby total protein staining, shows successful purification (C). Immunodetection with a Ub-specific antibody shows precipitation of polyubiquitinated (pUb) proteins (marked with a solid black line) (D), while HA-tag-specific immunodetection (E) demonstrates the presence of Ub forms of KICS2-WT and -fs (indicated by solid and dashed gray lines, respectively). GAPDH served as the loading control. The asterisk marks an unspecific protein band present in the input. Unmodified/non-Ub HA-KICS2-WT and -fs were detectable in both the IP:ctrl and IP:Ub lanes, likely due to non-specific or indirect binding of the protein, regardless of its modification status.

(legend continued on next page)

SZT2 and KPTN, we concluded that the frameshift leads to a virtual LOF. Furthermore, we included a LOF variant containing a homozygous frameshift in exon 3 of *SZT2* as a positive control for impaired KICSTOR complex activity.

To test KICSTOR-regulated mTORC1 signaling, we performed amino acid deprivation and re-supplementation in control and KICS2-modified cell lines. Western blot analysis of control cell lines demonstrated a significant decrease in mTORC1 activity upon amino acid deprivation for 1 h, as indicated by reduced phosphorylation of S6K at position Thr389, which has been shown previously.[1,2] This nutrient-dependent regulation of mTORC1 activity was significantly impaired in both homozygous LOF cell lines of SZT2 and KICS2, as well as in homozygous p.Tyr393Cys cells (Figure 4). These cells showed higher levels of S6K phosphorylation in amino-acid-free media but also in normal growth media. mTORC1 activity was additionally assessed by measuring the phosphorylation of 4EBP1 at Ser65. As expected, under amino acid starvation, wild-type cells did not exhibit phosphorylation of 4EBP1. In contrast, homozygous LOF cells of KICS2 and SZT2 showed highly phosphorylated 4EBP1. Both KICS2 missense variants appeared to have a similar but lesser effect on 4EBP1 Ser65 phosphorylation; only the changes in 4EBP1 phosphorylation in KICS2 and SZT2 LOF cells reached statistical significance. For 4EBP1, we detected two bands, with the higher band corresponding to phosphorylated 4EBP1. Consistent with this, mainly the lower band was detected in wild-type cells after amino acid deprivation. In both LOF cell lines, as well as the p.Tyr393Cys cells and, to some extent, the p.Asp296Glu cell line, both bands were detected also after amino acid deprivation.

Phosphoproteome analysis confirms mTORC1 dysregulation and suggests involvement of ciliogenesis

We next performed phosphoproteome analyses on control and modified HEK293T cells after 1 h of amino acid deprivation. For each cell line, we identified between 41 and 49 differentially phosphorylated proteins compared to wild-type cells (Table S5; Figure S4). In line with our previous observations, we found that nutrient-dependent mTORC1 activation was indeed impaired for all mutant cell lines: KICS2:p.Tyr393Cys, KICS2:p.Asp296Glu, KICS2 LOF, and SZT2 LOF (Figure 5). A pathway analysis using IPA revealed the most commonly dysregulated signaling pathways to be "mTOR signaling," "regulation of eIF4 and p70S6K," and "EIF2 signaling." Several other pathways involved in transcription, protein synthesis, mitosis, and glucose metabolism were also differentially phosphorylated in most of the samples analyzed.

Proteins whose phosphorylation was most affected by KICS2 and SZT2 included known regulators and downstream effectors of mTORC1. All mutant cell lines were differentially phosphorylated, compared to controls, for the following proteins: ILF3 is responsible for tethering the GATOR complexes to the lysosome for regulation of mTORC1.[48] EIF4G1 is a member of the EIF4F complex, which is a direct effector of mTORC1 that is essential for the initiation of translation.[49] EEF2 is a translation elongation factor,[50] and RPS6 is a component of the ribosome,[51] rendering both involved in translation. SRRM2 is involved in splicing speckle formation and mRNA splicing.[52] mTORC1 is a well-known regulator of translation and has been demonstrated to play a role in post-transcriptional regulation via splicing. SRRM2, eIF4G1, and RPS6 were previously demonstrated to be members of the mTORC1-regulated phosphoproteome.[53] Interestingly, *SRRM2* haploinsufficiency (MIM: 620439) causes intellectual disability,[54] *EIF4G1* is associated with Parkinson disease (MIM: 614251),[55] and *EEF2* mutations were identified in individuals with ataxia (MIM: 609306).[56]

Literature and database searches revealed that about 40% of the differentially phosphorylated proteins were part of the mTORC1 pathway, among them many members of the EIF4F complex. In accordance with this, we found that about 50% of the differentially phosphorylated proteins are involved in apoptosis, while about 80% of the proteins are involved in proliferation, two processes that are regulated by mTORC1. About 15% of the proteins are involved in transcription or translation, which reflects the findings of our pathway analysis. Interestingly, 50%–75% of the differentially phosphorylated proteins in this study are part of the ciliary or centrosomal proteome (Figure 5). Taken together, our phosphoproteomics analyses of modified HEK293T cells suggest that changes in translation, post-transcriptional regulation, and ciliogenesis may underlie the pathophysiology observed in individuals with pathogenic *KICS2* variants.

(F) Investigation of the proteolytic mechanism responsible for the degradation of WT KICS2 and, in particular, the KICS2 p.Lys260Asnfs*18 (KICS2-fs) variant. HEK293T cells expressing KICS2-WT and KICS2-fs, along with MYC-tagged KPTN and FLAG-tagged SZT2, were treated with the proteasome inhibitor epoxomicin (Epoxo) or autophagy inhibitor bafilomycin A1 (BafA1). DMSO served as the vehicle control. Western blot analysis confirms the accumulation of K48-linked pUb (K48-pUb) chains and LC3B-II as markers of successful proteasomal or autophagosomal inhibition, respectively. HA-tag-specific detection shows a strong accumulation of KICS2-WT and KICS2-fs, as well as their Ub forms (Ub-WT and Ub-fs), upon proteasomal, but not autophagosomal, inhibition. GAPDH served as the loading control. The asterisk marks an unspecific protein band.
(G) Relative quantification of KICS2 and Ub KICS2 amounts, relative to vehicle-treated control from $n = 3$ biological replicates, shows significantly increased levels upon proteasomal inhibition. Calculating the ratios between Ub-KICS2 and KICS2 shows that baseline ubiquitination of KICS-fs is significantly higher compared to KICS2-WT (****$p < 0.0001$, **$p < 0.01$, and *$p < 0.05$, one-sample t test and two-way ANOVA followed by Šídák's multiple comparison test).

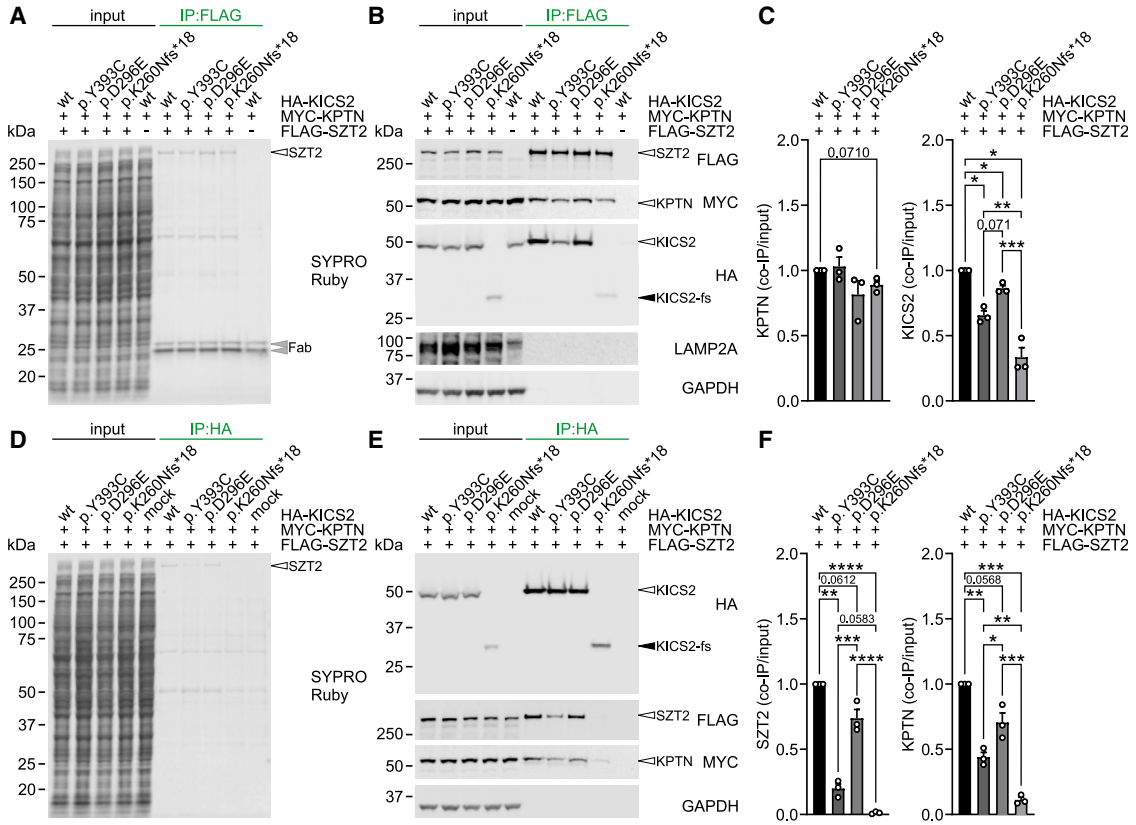

Figure 3. Missense and frameshift variants of KICS2 compromise the formation of the KICSTOR complex

(A and B) Interaction analysis of key components of the KICSTOR complex using FLAG-tag-specific co-immunoprecipitation (coIP) of lysates from HEK293T cells transfected with HA-tagged wild-type (WT) KICS2, its p.Tyr393Cys and p.Asp296Glu missense variants, or the truncated frameshift variant p.Lys260Asnfs*18 (KICS2-fs), along with MYC-tagged KPTN and FLAG-tagged SZT2, or an empty control vector (mock). SZT2 was purified via its FLAG tag together with its binding partners KICS2 and KPTN. Western blot analysis of input samples and eluates, followed by SYPRO Ruby total protein staining, shows successful purification and precipitation of FLAG-SZT2 (A). Gray arrowheads mark Fab bands. KPTN and KICS2-WT were co-purified as interaction partners of SZT2, while all three KICS2 variants showed diminished binding (B). The previously reported SZT2 interaction partner LAMP2A was not co-precipitated. Overexpressed proteins were detected using tag-specific antibodies. GAPDH served as the loading control.

(C) Relative quantification of co-precipitated MYC-KPTN and HA-KICS2, normalized to their expression levels, from $n = 3$ biological replicates. While KPTN binding was not influenced by the presence of the three KICS2 variants, all variants showed diminished binding to SZT2, with the KICS2-fs demonstrating the strongest reduction (***$p < 0.001$, **$p < 0.01$, and *$p < 0.05$, one-sample t test and two-way ANOVA followed by Tukey's multiple comparison test).

(D and E) The interaction analysis was validated using FLAG-tag-specific coIP of lysates from HEK293T cells transfected with HA-tagged WT KICS2, its p.Tyr393Cys and p.Asp296Glu missense variants, the truncated fs variant p.Lys260Asnfs*18 (KICS2-fs), or an empty control vector (mock), along with MYC-tagged KPTN and FLAG-tagged SZT2. HA-KICS2 was purified via its HA tag together with its binding partners SZT2 and KPTN. Western blot analysis of input samples and eluates, followed by SYPRO Ruby total protein staining, shows successful purification and co-precipitation of FLAG-SZT2 (D). SZT2 and KPTN were co-purified as interaction partners of WT KICS2, while interaction with all three KICS2 variants showed diminished binding or, in the case of SZT2 and the C-terminally truncated fs variant of KICS2, even an absence of interaction (E). Overexpressed proteins were detected using tag-specific antibodies. GAPDH served as the loading control.

(F) Relative quantification of co-precipitated FLAG-SZT2 and MYC-KPTN, normalized to their expression levels, from $n = 3$ biological replicates. STZ2 binding to KICS2 variants was strongly reduced for the p.Tyr393Cys variant and practically absent for the C-terminally truncated fs variant. KPTN binding was also reduced, though it was not absent in the case of KICS2-fs (****$p < 0.0001$, ***$p < 0.001$, **$p < 0.01$, and *$p < 0.05$, one-sample t test and two-way ANOVA followed by Tukey's multiple comparison test).

Zebrafish depleted of Kics2 corroborate its function in ciliogenesis and brain development

We turned to zebrafish embryos for an *in vivo* evaluation of the identified gene variants of *KICS2*. Zebrafish possess one *kics2* gene, which we found to be ubiquitously expressed during early zebrafish development. At later stages, it becomes enriched in neuronal structures as well as tissues harboring cilia (Figure S5). To knock down *kics2* in zebrafish, we turned to antisense MOs. In order to generate robust results, we made use of two different MOs: those interfering with translation (Kics2 ATG MOs) and splicing (Kics2 splMOs), respectively. The impact on splicing of the Kics2 splMO was first verified by RT-PCR (Figure S6). Injection of this MO resulted in embryos with edema and otolith defects (Figures 6A–6D). The same phenotype was observed after injection of the Kics2 ATG MO (Figure S7). Co-injection of capped RNA encoding human *KICS2* rescued phenotypes induced by Kics2 splMOs,

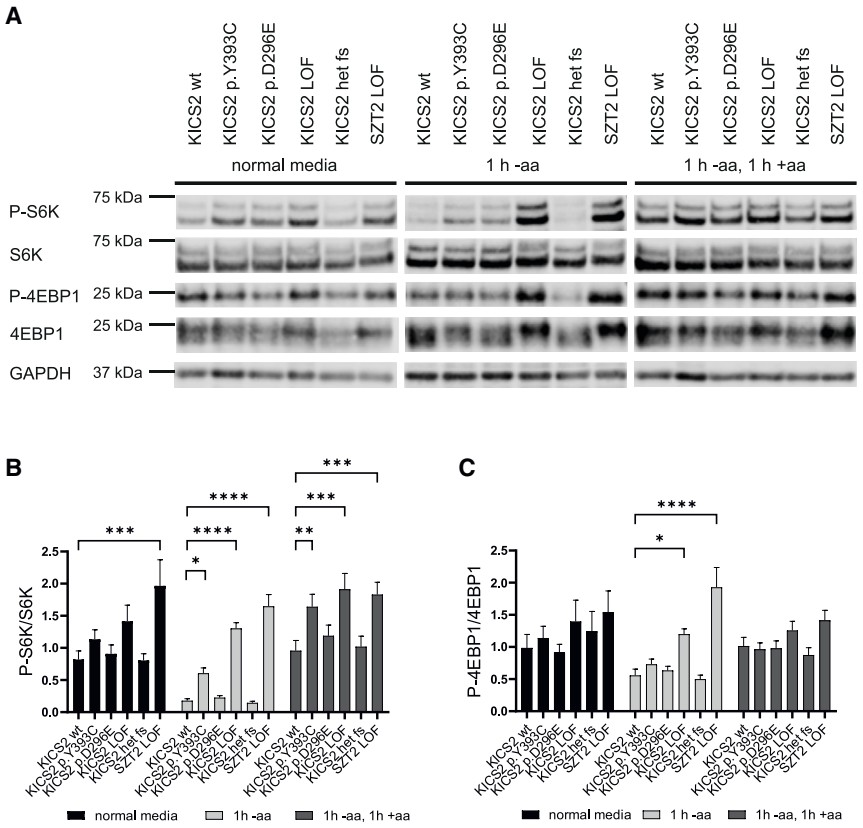

Figure 4. mTORC1 activity assay shows dysregulation of mTORC1 activity for the identified variants

(A) HEK293T cells (wild type [WT], loss of function [LOF], heterozygous for LOF variant [het fs], or indicated variants) were incubated either for 1 h in amino-acid-free media (−aa) or for 1 h in amino-acid-free media followed by 1 h of normal growth media (+aa). Cells without prior incubation in amino-acid-free media were used as baseline control. Western blots were performed, and the amounts of P-S6K, S6K, P-4EBP1, and 4EBP1 were measured; GAPDH served as a loading control. For 4EBP1, two bands were detected, with the higher band corresponding most likely to the phosphorylated 4EBP1. For both LOF cell lines as well as the p.Tyr393Cys and, to some extent, the p.Asp296Glu cell line, a shift in these two bands can be seen for amino-acid-free media compared to the WT cell line. Quantification of this shift was hindered by the closeness of the bands.

(B) Relative quantification of the changes in phosphorylation in S6K upon amino acid deprivation determined by the ratio of P-S6K and S6K in amino-acid-free media or normal growth media from $n = 7$ biological replicates (****$p < 0.0001$, ***$p < 0.001$, **$p < 0.01$, and *$p < 0.05$, two-way ANOVA followed by Dunnett's multiple comparison test).

(C) Relative quantification of the changes in phosphorylation in 4EBP1 upon amino acid deprivation determined by the ratio of P-4EBP1 and 4EBP1 in amino-acid-free media or normal growth media from $n = 7$ biological replicates (****$p < 0.0001$, ***$p < 0.001$, **$p < 0.01$, and *$p < 0.05$, two-way ANOVA followed by Dunnett's multiple comparison test).

underscoring the specificity of the latter. However, no rescue could be observed after co-injection of RNAs encoding any of the identified variants (Figures 6A–6D). Consistent with the reported role of human KICS2 in dampening mTOR signaling, knockdown embryos displayed brighter fluorescence when immunostained with a phospho-S6 antibody. Co-injection of RNA encoding human *KICS2* reduced the phospho-S6 signal, while RNA encoding a truncated variant did not (Figure S8). As deregulated mTOR signaling,[15] as well as both observed live phenotypes, may be indicative of cilia dysfunction,[57] we assessed left-right asymmetry development, which depends on functional cilia in the temporal organ of laterality, the Kupffer's vesicle.[15] Depletion of Kics2 via both MOs resulted in the same defects in organ placement (Figures 6E, 6F, and S7) and impaired left-right patterning, as shown for the leftward gene *spaw*. This further supports the hypothesis of KICS2 controlling cilia biology. Importantly, administration of rapamycin partially rescued *spaw* distribution, suggesting that KICS2 modulates cilia through the fine-tuning of mTOR activity (Figure 6G). To further corroborate this hypothesis, we analyzed cilia in the Kupffer's vesicle. Depletion of Kics2 resulted in elongated cilia compared to control embryos (Figure 6H). Expression of wild-type *KICS2* reduced cilium length to control levels, while the truncation variant p.Lys262* did not. Moreover, neuromast cilia as well as cilia in the developing pronephros were also longer upon Kics2 depletion (Figures S9A–S9D).

As a way to confirm a conserved function of KICS2, we also knocked down KICS2 in human fibroblasts and analyzed cilia in this heterologous cell model. Loss of KICS2 resulted in longer cilia, which could be normalized to control length by overexpression of zebrafish Kics2 but not by a variant resembling the truncation after lysine 260 (Figures S9 and S10).

Intriguingly, we also observed that *KICS2* expression must be very tightly regulated, as injection of larger amounts of capped RNA—as described for the rescue of the live phenotype (Figure 6)—led to the development of cyclopia resembling holoprosencephaly. Injection of the same amount of either identified variant, however, failed to induce this phenotype to the same extent wild-type KICS2 did (Figure S11). These data together demonstrate that the variants identified in affected individuals display impaired functionality toward mTOR signaling, as well as cilia and brain development.

In summary, we identified bi-allelic variants in *KICS2* in 8 families. All affected individuals presented with intellectual disability sometimes accompanied by epilepsy or

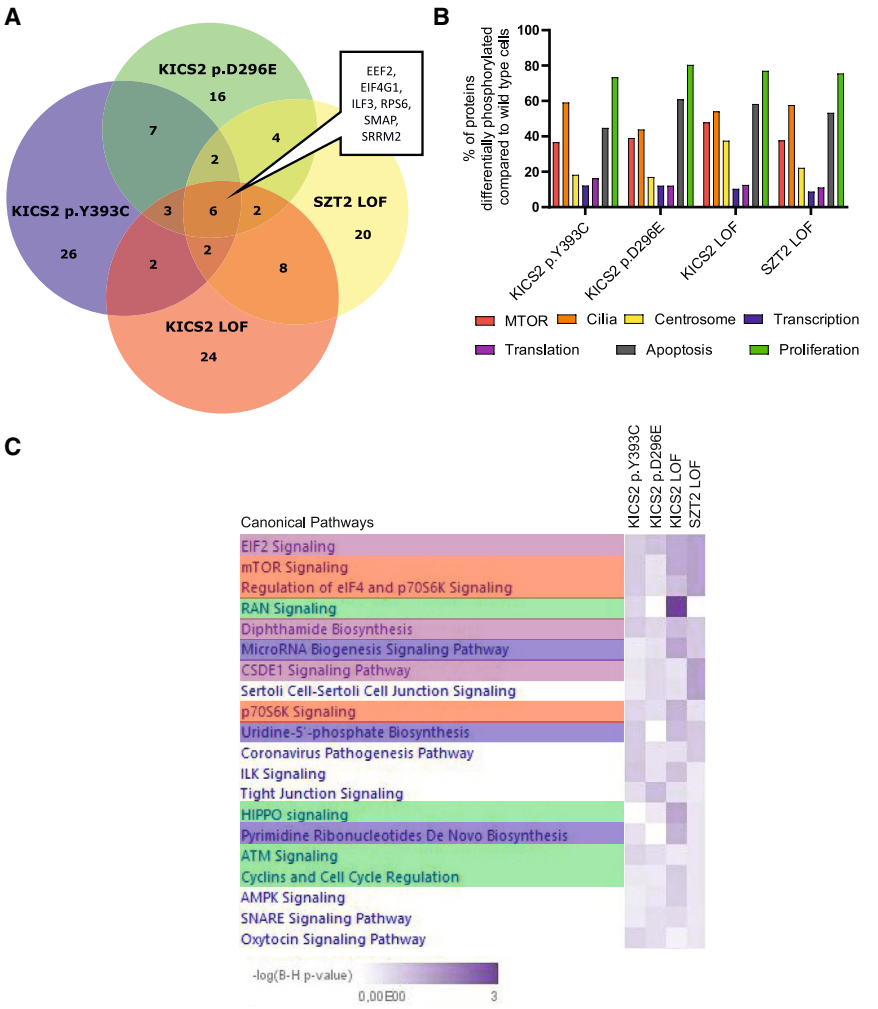

Figure 5. Phosphoproteome data reveal differentially phosphorylated proteins linked to cilia and the centrosome
(A) Number of differentially phosphorylated proteins compared to wild-type cells per sample and overlap between samples.
(B) Percentage of proteins associated with cellular processes (mTOR, cilia, centrosome, transcription, translation, apoptosis, and proliferation) that are differentially phosphorylated when compared to wild-type cells.
(C) Pathway analysis using IPA indicates changes in several pathways associated with mTOR activity (red), transcription (blue), translation (violet), and proliferation (green). Only the top 20 signaling pathways are shown.

hearing impairment. Our cell culture models showed a significant effect of the identified variants on KICSTOR complex formation and nutrient-dependent mTORC1 activity—similar to what was seen for individuals with biallelic variants in another KICSTOR protein component, SZT2.[58] Experiments in zebrafish established that the identified variants exhibit inferior functionality compared to wild-type KICS2.

Discussion

Dysregulation of mTORC1 activity has been shown to cause a variety of disorders, including intellectual disability.[3–8] Many of these disorders have also been associated with epilepsy and macrocephaly, such as Cowden syndrome (*PTEN* [MIM: 158350]) or Smith-Kingsmore syndrome (*MTOR* [MIM: 616638]). These phenotypes have also been described for individuals with defects in KICSTOR components *SZT2* and *KPTN* (MIM: 615476 and 615637).[9,10] All individuals with *KICS2* variants examined here showed intellectual disability, but epilepsy and hearing impairment were only observed in 8 and 3 individuals, respectively. Although most probands in this study generally had high normal head circumferences, only two of them had (relative) macrocephaly. In summary, while all individuals with defects in KICSTOR complex components reported to date share intellectual disability as a common feature, there appears to be phenotypic variability between individuals with *SZT2* or *KPTN* variants and those with *KICS2* variants.

When analyzing protein levels of KICS2 with either one of the missense variants or the p.Lys260Asnfs*18 variant in an overexpression cell model, the truncating frameshift variant showed a decreased protein stability corresponding to a LOF effect. The reduced levels could be attributed to an

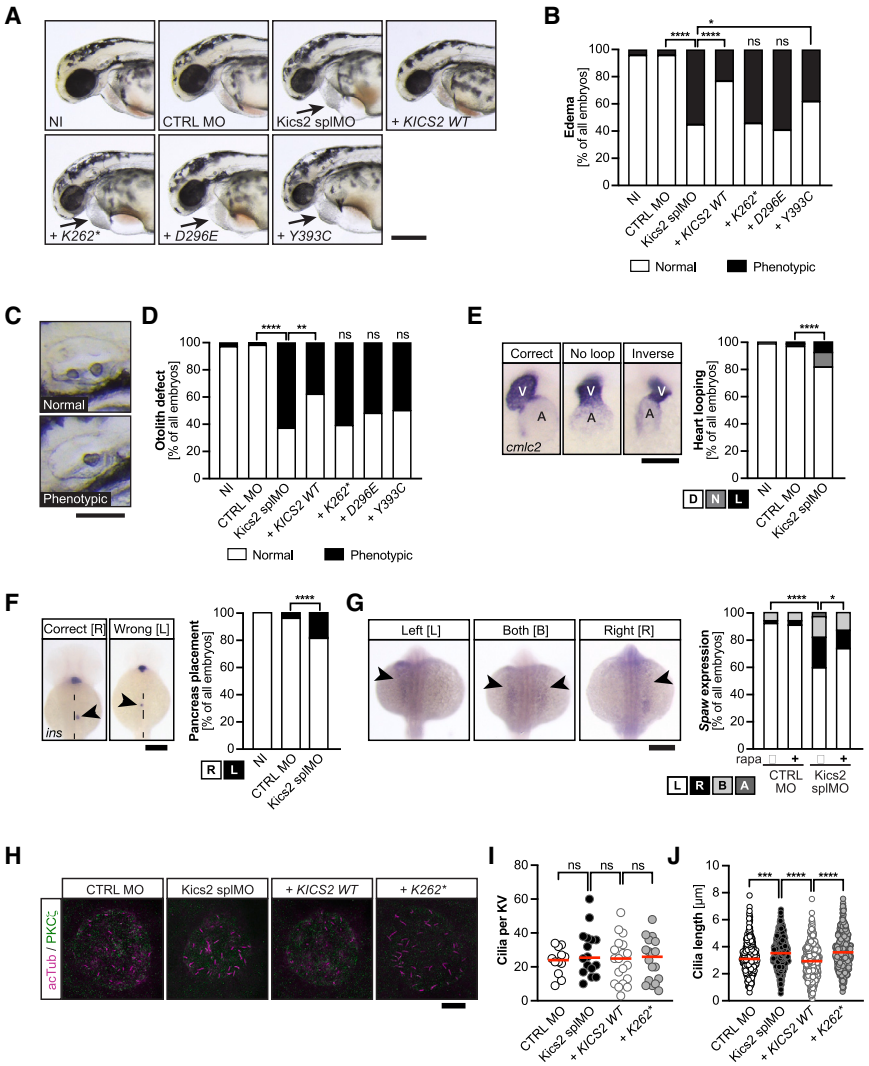

Figure 6. Kics2 loss-of-function impacts on embryonic development and cilium functionality

(A) Kics2 depletion results in edema formation, which is not rescued by variants identified in this study. Live zebrafish at 48 hpf. Arrow indicates edema. NI, non-injected; CTRL MO, control MO; + *KICS2 WT*, + *K262**, + *D296E*, + *Y393C*, embryos co-injected with Kics2 splMO and capped RNA encoding human *KICS2* WT or identified variants. Scale bar: 300 μm.

(B) Stacked bar graph of edema formation summarizing 7 experiments with 77–121 embryos in total. Two-tailed Fisher's exact test. ****$p < 0.0001$, *$p = 0.035$, and ns: $p > 0.05$.

(C) Loss of Kics2 function leads to defective otolith seeding at 48 hpf. Scale bar: 100 μm.

(D) Stacked bar graph summarizing otolith defects in 7 experiments with 77–121 embryos in total. Two-tailed Fisher's exact test. ****$p < 0.0001$, **$p = 0.0018$, and ns: $p > 0.05$.

(E) Kics2 depletion affects heart looping. Images of *cmcl2 in situ* hybridization at 48 hpf (scale bar: 100 μm; A, atrium; V, ventricle). Graph displays correct (D), unlooped (N), and inversely (L) looped hearts. Two-tailed Fisher's exact test. ****$p < 0.0001$. 8 experiments with 220–239 embryos.

(F) *Insulin* (*ins*) *in situ* hybridization to detect pancreas localization. Dashed line: midline. Scale bar: 200 μm. Graph displays correctly (R) and wrongly (L) placed pancreata. Two-tailed Fisher's exact test. ****$p < 0.0001$. 8 experiments with 221–238 embryos.

(G) *Southpaw* (*spaw*) expression is randomized upon *kics2* knockdown but can be partially rescued by rapamycin treatment. Arrowheads: expression in the lateral plate mesoderm. Scale bar: 200 μm. Two-tailed Fisher's exact test. ****$p < 0.0001$ and *$p = 0.0341$. 5 experiments with 109–120 embryos.

(H) Confocal stacks of 6 somite stage Kupffer's vesicles (KVs) stained for acetylated tubulin (acTub; magenta) and PKCζ (green). Scale bar: 20 μm.

(I) Kics2 manipulation does not affect the number of cilia per KV. 2 experiments with 12–19 embryos. Kruskal-Wallis test with Dunn's multiple comparison test. ns: $p > 0.05$.

(J) KV cilia become elongated upon loss of Kics2 function. 2 experiments with 135–323 cilia. Kruskal-Wallis test with Dunn's multiple comparison test. ****$p < 0.0001$ and ***$p = 0.001$.

increase in ubiquitination and enhanced protein degradation of the *KICS2* frameshift variant via the UPS, demonstrating a proteostatic regulatory element upstream of KICSTOR signaling.

Investigating the repercussions of *KICS2* variants on the protein binding to known components of the KICSTOR complex via coIP showed that mutant forms of KICS2 exhibited significantly lower interactions with SZT2 and KPTN, which were nearly abolished for the frameshift variant. These observations substantiate that all investigated variants lead to a LOF effect. Furthermore, the more pronounced decrease in interaction for the p.Tyr393Cys variant compared to p.Asp296Glu suggests that C-terminal region of KICS2 likely harbors the binding motif to SZT2, the linker protein that mediates KICSTOR assembly and interaction with GATOR1.[1] Moreover, while we found that the interaction of wild-type KICS2 and KPTN is indeed severely impaired in the absence of SZT2, some reduced binding remained, suggesting a direct interaction between KPTN and perhaps the N-terminal part of KICS2. This direct interaction is further supported by an earlier MS-based interactome study, which detected KPTN as a binding partner of KICS2.[59] Further investigations are needed to explore the potential interaction between these two components of the KICSTOR complex and its regulatory repercussions on the linked pathway.

CRISPR-based modeling of all identified missense variants in HEK293T cells as well as LOF variants of KICS2 and SZT2 and testing for mTORC1 activity demonstrated a significant increase in S6K activity under amino acid

deprivation for KICS2 and SZT2 LOF variants as well as the p.Tyr393Cys variant. These findings are in line with a previous study on the effect of KICSTOR component depletion in HEK293T cells, which showed an impairment in the regulation of mTORC1 activity for all KICSTOR components.[1] Furthermore, a significant increase in S6K activity could be observed for these cell lines even under normal conditions, which is concordant with previous findings.[12] For 4EBP1, we could also see significant changes in phosphorylation for both LOF cell lines. Additionally, we could see a consistent shift in both detected bands for both LOF cell lines, the p.Tyr393Cys variant, and, to some extent, the p.Asp296Glu cell line. This indicates an effect on 4EBP1 phosphorylation also for both missense variants. Our subsequent phosphoproteome analysis also demonstrated a significant dysregulation of mTORC1 activity, aberrant phosphorylation of proteins involved in translation, post-transcriptional regulation (splicing), and ciliogenesis. We also observed abnormal phosphorylation in an upstream modulator of mTORC1, ILF3.[48]

Our phosphoproteomic analysis showed the same tendency in all mutant cell lines for most phosphorylation sites. Literature research on the differentially phosphorylated proteins revealed that a large percentage are involved in crucial pathways and processes, such as mTOR, transcription, translation, apoptosis, and proliferation, highlighting the importance of KICS2 and the KICSTOR complex. Our pathway analysis likewise highlighted these processes. Since the KICSTOR complex was previously shown to regulate mTORC1[1,12] and mTORC1 is known to regulate translation and cell growth,[60] an indirect effect on these processes via mTORC1 is likely. Interestingly, about half of the differentially phosphorylated proteins in all KICS2 cell lines were cilia proteins, while another 17%–37% were centrosome proteins. Up to now, there has been no report of a direct effect of KICS2 on ciliogenesis, whereas SZT2 has already been associated with cilia biology.[13] When analyzing human fibroblasts, however, we established a function of KICS2 in cilia biology. Although the precise mechanism remains to be uncovered and will be the focus of subsequent studies, it is very likely that KICS2 regulates cilia through mTOR. The reciprocal regulation between mTORC1 and primary cilia has been well established.[61] While primary cilia downregulate mTORC1 activity in quiescent cells,[62] the activation of mTORC1 promotes longer cilia.[63] Since KICS2 acts as a negative regulator of mTOR signaling and elevated mTOR activity precipitates in longer cilia,[43,64] we conclude that dysfunction of KICS2 likely facilitates normal cilia formation by fine-tuning mTOR activity. Alternatively, several differentially phosphorylated proteins have previously been associated with cilia dysfunction. These included tubulin as one major building block of cilia as well as proteins regulating microtubule dynamics. We also found a change in RAB8A, which traffics important signaling molecules to cilia,[65] and MCM2, which is required for cilium elongation.[66] Moreover, several of the phosphorylated proteins modulate centrosome homeostasis. As one of the centrioles of the centrosome becomes the basal body of the cilium once a cell exits the cell cycle,[67] it is possible that centrosome defects also contribute to the cilia phenotypes in the context of KICS2 LOF.

To strengthen this link between KICS2 and cilia, we used zebrafish, which are exceptionally well suited for the analysis of cilia-related phenomena. One of the best-studied developmental processes that depends on functional cilia in zebrafish is the development of the asymmetric arrangement of internal organs. Loss or dysfunction of those cilia, which mediate left-right asymmetry development, results in situs anomalies, which can be assessed on the level of heart looping, abdominal organ placement, and the expression of leftward genes in the lateral plate mesoderm. Our experiments clearly show that KICS2 controls asymmetry development through these cilia and that at least the truncation variant identified in affected individuals has lost this control over cilia. This does not mean, however, that individuals carrying *KICS2* variants, or such variants in other KICSTOR complex components, suffer from situs anomalies, too. To draw such a conclusion, a considerably larger number of affected individuals would need to be examined. Some individuals with variants in *DEPDC5* (MIM: 620504) showed defects of the eye or heart, which could be caused by ciliary defects.[68] Moreover, in our cohort, we observed clinodactyly in one individual and hearing disability in 3 affected individuals, which might be caused by cilia defects.

So far, the phenotypic discrepancy between zebrafish, fibroblasts, and individuals with defects in mTORC1 activity cannot be fully explained yet, but our phenotypic findings in the affected individuals and zebrafish are consistent with the results of others for the respective species. Our assays show a discrepancy between the effects of the different variants. While truncating variants show an almost complete LOF effect, the p.Tyr393Cys variant retains some interaction with SZT2 and KPTN as well as about 50% rest function in the mTORC1 activity assay. For the p.Asp296Glu variant, the mTORC1 assay was not significant, and the interaction is only decreased by about 20%. Since we identified the p.Asp296Glu variant only in one individual and the data are ambiguous, one could argue that this variant remains a variant of unknown significance. However, for the p.Tyr393Cys variant, our evidence is much better, with two unrelated families affected and significance for all assays. Still, we cannot see a more severe phenotype for the truncating variants in affected individuals compared to individuals with missense variants. One reason could be the observed dosage effect in our zebrafish models. Here, we found that already a small change in *kics2* concentration, whether an increase or decrease, can cause a phenotype like holoprosencephaly. This suggests that subtle variations in KICSTOR complex composition or dosage are sufficient to trigger changes in brain development and, therefore, can cause intellectual disability.

Here, we report on 11 individuals of 8 families carrying bi-allelic variants in *KICS2*. Our functional studies using cell culture and zebrafish show decreased stability of the KICS2 frameshift variant, compromised binding of mutant forms of KICS2 to components of the KICSTOR complex, impairment in the regulation of mTORC1 activity, and a LOF defect for both homozygous missense variants. We substantiated a defect in ciliogenesis, which further highlights the relevance of KICS2 as a member of the KICSTOR complex. Overall, we establish that pathogenic variants in *KICS2* can cause intellectual disability. Given its role in mTOR regulation, therapy with mTOR modifiers may be an option worth exploring in the future.

Data and code availability

This study did not generate new code. Sequence datasets have been generated and contributed by different study sites and have not been deposited in a public repository due to varying local consent regulations. Selected datasets, such as read count data from RNA sequencing (RNA-seq), might be available from the corresponding author upon request.

Acknowledgments

We would like to thank the families for taking part in the study. Furthermore, we would like to thank the animal caretakers at University Hospital Tübingen for excellent fish care and Melanie Tingler for assistance with cloning. We are further grateful for additional grant support by the German Academic Exchange Service (DAAD) as part of the German-Arab Transformation Program Line 4 (project ID 57166498), the Fundació la Marató de TV3 (grant number 202019-32), and the Deutsche Forschungsgemeinschaft (German Research Foundation, DFG, grant numbers PH144/4-3, PH144/6-1, and 467868420 to M.P.; 418081722 and 433158657 to T.B.H.; FOR2715 [Le1030/16-1, Le1030/16-2, We4896/4-1, and We4896/4-2] to H.L. and Y.W.; WE 6585/1-1 to J.J.W.; and INST 37/1049-1 to O.R.). R.B. was supported by Deutsche Forschungsgemeinschaft (German Research Foundation, DFG, grant number BU 3602/1-1). T.B.H. was supported by the European Commission (Recon4IMD - GAP-101080997). P.E.B. was awarded NIH NINDS RO1 NS08372. UCL families were collected as part of the SYNaPS Study Group collaboration funded by the Wellcome Trust and strategic award (Synaptopathies) funding (WT093205 MA and WT104033AIA), and research was conducted as part of the Queen Square Genomics group at University College London, supported by the National Institute for Health Research University College London Hospitals Biomedical Research Centre. S.E. and H.H. were supported by an MRC strategic award to establish an International Centre for Genomic Medicine in Neuromuscular Diseases (ICGNMD) MR/S005021/1. Family E was identified via access to data in the National Genomic Research Library via the Genomics England Research Environment.

Author contributions

R.B., M.D.B., M.P., and T.B.H. designed the experiments. R.B., K.C., S.E., R.K., L.M., R.M., M.H.-E., M.K., J.P., H.E., H.H., A.T.P., Y.W., P.E.B., O.R., and T.B.H. performed genetic studies. T.R., K.C., J.R.A., T.F., S.G., U.G., S.S., M.H., T.S., H.L., A.T.P., I.B., and P.E.B. performed phenotyping or collected clinical data. M.S. performed the bioinformatic analysis. R.B., L.S., M.D.B., and D.K. performed and analyzed cell culture experiments. M.D.B. and M.P. performed and analyzed zebrafish experiments. C.H. and J.J.W. performed cell-culture-based overexpression and coIP experiments. A.V. performed MS. R.B., M.D.B., J.J.W., M.P., and T.B.H. wrote the initial version of the manuscript. All authors contributed to the review/editing of the manuscript.

Declaration of interests

The authors declare no competing interests.

Web resources

Cildb, http://cildb.i2bc.paris-saclay.fr/
Combined Annotation Dependent Depletion 23, https://cadd.gs.washington.edu
DeepVenn, http://www.deepvenn.com/
Ensembl Variant Effect Predictor, https://ensembl.org/Homo_sapiens/Tools/VEP
gnomAD server, https://gnomad.broadinstitute.org
Online Mendelian Inheritance in Man (OMIM), https://www.omim.org
PubMed, https://pubmed.ncbi.nlm.nih.gov/

Supplemental information

Supplemental information can be found online at https://doi.org/10.1016/j.ajhg.2024.12.019.

Received: June 18, 2024
Accepted: December 19, 2024
Published: January 16, 2025

References

1. Wolfson, R.L., Chantranupong, L., Wyant, G.A., Gu, X., Orozco, J.M., Shen, K., Condon, K.J., Petri, S., Kedir, J., Scaria, S.M., et al. (2017). KICSTOR recruits GATOR1 to the lysosome and is necessary for nutrients to regulate mTORC1. Nature *543*, 438–442. https://doi.org/10.1038/nature21423.
2. Peng, M., Yin, N., and Li, M.O. (2017). SZT2 dictates GATOR control of mTORC1 signalling. Nature *543*, 433–437. https://doi.org/10.1038/nature21378.
3. Ricos, M.G., Hodgson, B.L., Pippucci, T., Saidin, A., Ong, Y.S., Heron, S.E., Licchetta, L., Bisulli, F., Bayly, M.A., Hughes, J., et al. (2016). Mutations in the mammalian target of rapamycin pathway regulators NPRL2 and NPRL3 cause focal epilepsy. Ann. Neurol. *79*, 120–131. https://doi.org/10.1002/ana.24547.
4. Scheffer, I.E., Phillips, H.A., O'Brien, C.E., Saling, M.M., Wrennall, J.A., Wallace, R.H., Mulley, J.C., and Berkovic, S.F. (1998). Familial partial epilepsy with variable foci: a new partial epilepsy syndrome with suggestion of linkage to chromosome 2. Ann. Neurol. *44*, 890–899. https://doi.org/10.1002/ana.410440607.
5. Baynam, G., Overkov, A., Davis, M., Mina, K., Schofield, L., Allcock, R., Laing, N., Cook, M., Dawkins, H., and Goldblatt, J. (2015). A germline MTOR mutation in Aboriginal Australian siblings with intellectual disability, dysmorphism,

macrocephaly, and small thoraces. Am. J. Med. Genet. *167*, 1659–1667. https://doi.org/10.1002/ajmg.a.37070.
6. Liaw, D., Marsh, D.J., Li, J., Dahia, P.L., Wang, S.I., Zheng, Z., Bose, S., Call, K.M., Tsou, H.C., Peacocke, M., et al. (1997). Germline mutations of the PTEN gene in Cowden disease, an inherited breast and thyroid cancer syndrome. Nat. Genet. *16*, 64–67. https://doi.org/10.1038/ng0597-64.
7. Kumar, A., Wolpert, C., Kandt, R.S., Segal, J., Pufky, J., Roses, A.D., Pericak-Vance, M.A., and Gilbert, J.R. (1995). A de novo frame-shift mutation in the tuberin gene. Hum. Mol. Genet. *4*, 1471–1472. https://doi.org/10.1093/hmg/4.8.1471.
8. van Slegtenhorst, M., de Hoogt, R., Hermans, C., Nellist, M., Janssen, B., Verhoef, S., Lindhout, D., van den Ouweland, A., Halley, D., Young, J., et al. (1997). Identification of the tuberous sclerosis gene TSC1 on chromosome 9q34. Science *277*, 805–808. https://doi.org/10.1126/science.277.5327.805.
9. Baple, E.L., Maroofian, R., Chioza, B.A., Izadi, M., Cross, H.E., Al-Turki, S., Barwick, K., Skrzypiec, A., Pawlak, R., Wagner, K., et al. (2014). Mutations in KPTN cause macrocephaly, neurodevelopmental delay, and seizures. Am. J. Hum. Genet. *94*, 87–94. https://doi.org/10.1016/j.ajhg.2013.10.001.
10. Basel-Vanagaite, L., Hershkovitz, T., Heyman, E., Raspall-Chaure, M., Kakar, N., Smirin-Yosef, P., Vila-Pueyo, M., Kornreich, L., Thiele, H., Bode, H., et al. (2013). Biallelic SZT2 mutations cause infantile encephalopathy with epilepsy and dysmorphic corpus callosum. Am. J. Hum. Genet. *93*, 524–529. https://doi.org/10.1016/j.ajhg.2013.07.005.
11. Saleh, S., Beyyumi, E., Al Kaabi, A., Hertecant, J., Barakat, D., Al Dhaheri, N.S., Al-Gazali, L., and Al Shamsi, A. (2021). Spectrum of neuro-genetic disorders in the United Arab Emirates national population. Clin. Genet. *100*, 573–600. https://doi.org/10.1111/cge.14044.
12. Nakamura, Y., Kato, K., Tsuchida, N., Matsumoto, N., Takahashi, Y., and Saitoh, S. (2019). Constitutive activation of mTORC1 signaling induced by biallelic loss-of-function mutations in SZT2 underlies a discernible neurodevelopmental disease. PLoS One *14*, e0221482. https://doi.org/10.1371/journal.pone.0221482.
13. Cattelani, C., Lesiak, D., Liebscher, G., Singer, I.I., Stasyk, T., Wallnöfer, M.H., Heberle, A.M., Corti, C., Hess, M.W., Pfaller, K., et al. (2021). The SZT2 Interactome Unravels New Functions of the KICSTOR Complex. Cells *10*, 2711. https://doi.org/10.3390/cells10102711.
14. Condon, K.J., and Sabatini, D.M. (2019). Nutrient regulation of mTORC1 at a glance. J. Cell Sci. *132*, jcs222570. https://doi.org/10.1242/jcs.222570.
15. Casar Tena, T., Burkhalter, M.D., and Philipp, M. (2015). Left-right asymmetry in the light of TOR: An update on what we know so far. Biol. Cell *107*, 306–318. https://doi.org/10.1111/boc.201400094.
16. Suciu, S.K., and Caspary, T. (2021). Cilia, neural development and disease. Semin. Cell Dev. Biol. *110*, 34–42. https://doi.org/10.1016/j.semcdb.2020.07.014.
17. Ebrahimi-Fakhari, D., Saffari, A., Wahlster, L., Lu, J., Byrne, S., Hoffmann, G.F., Jungbluth, H., and Sahin, M. (2016). Congenital disorders of autophagy: an emerging novel class of inborn errors of neuro-metabolism. Brain *139*, 317–337. https://doi.org/10.1093/brain/awv371.
18. Han, C., Alkhater, R., Froukh, T., Minassian, A.G., Galati, M., Liu, R.H., Fotouhi, M., Sommerfeld, J., Alfrook, A.J., Marshall, C., et al. (2016). Epileptic Encephalopathy Caused by Mutations in the Guanine Nucleotide Exchange Factor DENND5A. Am. J. Hum. Genet. *99*, 1359–1367. https://doi.org/10.1016/j.ajhg.2016.10.006.
19. Mencacci, N.E., Kamsteeg, E.J., Nakashima, K., R'Bibo, L., Lynch, D.S., Balint, B., Willemsen, M.A.A.P., Adams, M.E., Wiethoff, S., Suzuki, K., et al. (2016). De Novo Mutations in PDE10A Cause Childhood-Onset Chorea with Bilateral Striatal Lesions. Am. J. Hum. Genet. *98*, 763–771. https://doi.org/10.1016/j.ajhg.2016.02.015.
20. Falb, R.J., Müller, A.J., Klein, W., Grimmel, M., Grasshoff, U., Spranger, S., Stöbe, P., Gauck, D., Kuechler, A., Dikow, N., et al. (2023). Bi-allelic loss-of-function variants in KIF21A cause severe fetal akinesia with arthrogryposis multiplex. J. Med. Genet. *60*, 48–56. https://doi.org/10.1136/jmedgenet-2021-108064.
21. Efthymiou, S., Salpietro, V., Malintan, N., Poncelet, M., Kriouile, Y., Fortuna, S., De Zorzi, R., Payne, K., Henderson, L.B., Cortese, A., et al. (2019). Biallelic mutations in neurofascin cause neurodevelopmental impairment and peripheral demyelination. Brain *142*, 2948–2964. https://doi.org/10.1093/brain/awz248.
22. Epi25 Collaborative Electronic address sberkovic@unimelbeduau; and Epi25 Collaborative (2019). Ultra-Rare Genetic Variation in the Epilepsies: A Whole-Exome Sequencing Study of 17,606 Individuals. Am. J. Hum. Genet. *105*, 267–282. https://doi.org/10.1016/j.ajhg.2019.05.020.
23. Hengel, H., Hannan, S.B., Dyack, S., MacKay, S.B., Schatz, U., Fleger, M., Kurringer, A., Balousha, G., Ghanim, Z., Alkuraya, F.S., et al. (2021). Bi-allelic loss-of-function variants in BCAS3 cause a syndromic neurodevelopmental disorder. Am. J. Hum. Genet. *108*, 1069–1082. https://doi.org/10.1016/j.ajhg.2021.04.024.
24. Smedley, D., Smith, K.R., Martin, A., Thomas, E.A., McDonagh, E.M., Cipriani, V., Ellingford, J.M., Arno, G., Tucci, A., et al.; 100000 Genomes Project Pilot Investigators (2021). 100,000 Genomes Pilot on Rare-Disease Diagnosis in Health Care - Preliminary Report. N. Engl. J. Med. *385*, 1868–1880. https://doi.org/10.1056/NEJMoa2035790.
25. Abou Jamra, R., Philippe, O., Raas-Rothschild, A., Eck, S.H., Graf, E., Buchert, R., Borck, G., Ekici, A., Brockschmidt, F.F., Nöthen, M.M., et al. (2011). Adaptor protein complex 4 deficiency causes severe autosomal-recessive intellectual disability, progressive spastic paraplegia, shy character, and short stature. Am. J. Hum. Genet. *88*, 788–795. https://doi.org/10.1016/j.ajhg.2011.04.019.
26. Schafgen, J., Cremer, K., Becker, J., Wieland, T., Zink, A.M., Kim, S., Windheuser, I.C., Kreiss, M., Aretz, S., Strom, T.M., et al. (2016). De novo nonsense and frameshift variants of TCF20 in individuals with intellectual disability and postnatal overgrowth. Eur. J. Hum. Genet. *24*, 1739–1745. https://doi.org/10.1038/ejhg.2016.90.
27. Sobreira, N., Schiettecatte, F., Valle, D., and Hamosh, A. (2015). GeneMatcher: a matching tool for connecting investigators with an interest in the same gene. Hum. Mutat. *36*, 928–930. https://doi.org/10.1002/humu.22844.
28. Sobreira, N., Schiettecatte, F., Boehm, C., Valle, D., and Hamosh, A. (2015). New tools for Mendelian disease gene identification: PhenoDB variant analysis module; and GeneMatcher, a web-based tool for linking investigators with an interest in the same gene. Hum. Mutat. *36*, 425–431. https://doi.org/10.1002/humu.22769.
29. Deschauer, M., Hengel, H., Rupprich, K., Kreiß, M., Schlotter-Weigel, B., Grimmel, M., Admard, J., Schneider, I., Alhaddad,

B., Gazou, A., et al. (2021). Bi-allelic truncating mutations in VWA1 cause neuromyopathy. Brain *144*, 574–583. https://doi.org/10.1093/brain/awaa418.
30. Weber, J.J., Czisch, L., Pereira Sena, P., Fath, F., Huridou, C., Schwarz, N., Incebacak Eltemur, R.D., Würth, A., Weishäupl, D., Döcker, M., et al. (2024). The parkin V380L variant is a genetic modifier of Machado-Joseph disease with impact on mitophagy. Acta Neuropathol. *148*, 14. https://doi.org/10.1007/s00401-024-02762-6.
31. Ran, F.A., Hsu, P.D., Wright, J., Agarwala, V., Scott, D.A., and Zhang, F. (2013). Genome engineering using the CRISPR-Cas9 system. Nat. Protoc. *8*, 2281–2308. https://doi.org/10.1038/nprot.2013.143.
32. Koblan, L.W., Doman, J.L., Wilson, C., Levy, J.M., Tay, T., Newby, G.A., Maianti, J.P., Raguram, A., and Liu, D.R. (2018). Improving cytidine and adenine base editors by expression optimization and ancestral reconstruction. Nat. Biotechnol. *36*, 843–846. https://doi.org/10.1038/nbt.4172.
33. Perez-Pinera, P., Kocak, D.D., Vockley, C.M., Adler, A.F., Kabadi, A.M., Polstein, L.R., Thakore, P.I., Glass, K.A., Ousterout, D.G., Leong, K.W., et al. (2013). RNA-guided gene activation by CRISPR-Cas9-based transcription factors. Nat. Methods *10*, 973–976. https://doi.org/10.1038/nmeth.2600.
34. Zittlau, K.I., Lechado-Terradas, A., Nalpas, N., Geisler, S., Kahle, P.J., and Macek, B. (2022). Temporal Analysis of Protein Ubiquitylation and Phosphorylation During Parkin-Dependent Mitophagy. Mol. Cell. Proteomics *21*, 100191. https://doi.org/10.1016/j.mcpro.2021.100191.
35. Boersema, P.J., Raijmakers, R., Lemeer, S., Mohammed, S., and Heck, A.J.R. (2009). Multiplex peptide stable isotope dimethyl labeling for quantitative proteomics. Nat. Protoc. *4*, 484–494. https://doi.org/10.1038/nprot.2009.21.
36. Cox, J., and Mann, M. (2008). MaxQuant enables high peptide identification rates, individualized p.p.b.-range mass accuracies and proteome-wide protein quantification. Nat. Biotechnol. *26*, 1367–1372. https://doi.org/10.1038/nbt.1511.
37. Tyanova, S., Temu, T., Sinitcyn, P., Carlson, A., Hein, M.Y., Geiger, T., Mann, M., and Cox, J. (2016). The Perseus computational platform for comprehensive analysis of (prote)omics data. Nat. Methods *13*, 731–740. https://doi.org/10.1038/nmeth.3901.
38. Kramer, A., Green, J., Pollard, J., Jr., and Tugendreich, S. (2014). Causal analysis approaches in Ingenuity Pathway Analysis. Bioinformatics *30*, 523–530. https://doi.org/10.1093/bioinformatics/btt703.
39. Arnaiz, O., Cohen, J., Tassin, A.M., and Koll, F. (2014). Remodeling Cildb, a popular database for cilia and links for ciliopathies. Cilia *3*, 9. https://doi.org/10.1186/2046-2530-3-9.
40. Arnaiz, O., Malinowska, A., Klotz, C., Sperling, L., Dadlez, M., Koll, F., and Cohen, J. (2009). Cildb: a knowledgebase for centrosomes and cilia. Database *2009*, bap022. https://doi.org/10.1093/database/bap022.
41. Hulsen, T., de Vlieg, J., and Alkema, W. (2008). BioVenn - a web application for the comparison and visualization of biological lists using area-proportional Venn diagrams. BMC Genom. *9*, 488. https://doi.org/10.1186/1471-2164-9-488.
42. Tena, T.C., and Philipp, M. (2016). Assessing Smoothened-mediated Hedgehog signaling in zebrafish. Methods Cell Biol. *132*, 147–164. https://doi.org/10.1016/bs.mcb.2015.10.001.
43. Gerhards, J., Maerz, L.D., Matthees, E.S.F., Donow, C., Moepps, B., Premont, R.T., Burkhalter, M.D., Hoffmann, C., and Philipp, M. (2023). Kinase Activity Is Not Required for G Protein-Coupled Receptor Kinase 4 Restraining mTOR Signaling during Cilia and Kidney Development. J. Am. Soc. Nephrol. *34*, 590–606. https://doi.org/10.1681/ASN.0000000000000082.
44. Burkhalter, M.D., Fralish, G.B., Premont, R.T., Caron, M.G., and Philipp, M. (2013). Grk5l controls heart development by limiting mTOR signaling during symmetry breaking. Cell Rep. *4*, 625–632. https://doi.org/10.1016/j.celrep.2013.07.036.
45. Longair, M.H., Baker, D.A., and Armstrong, J.D. (2011). Simple Neurite Tracer: open source software for reconstruction, visualization and analysis of neuronal processes. Bioinformatics *27*, 2453–2454. https://doi.org/10.1093/bioinformatics/btr390.
46. Lek, M., Karczewski, K.J., Minikel, E.V., Samocha, K.E., Banks, E., Fennell, T., O'Donnell-Luria, A.H., Ware, J.S., Hill, A.J., Cummings, B.B., et al. (2016). Analysis of protein-coding genetic variation in 60,706 humans. Nature *536*, 285–291. https://doi.org/10.1038/nature19057.
47. Go, C.D., Knight, J.D.R., Rajasekharan, A., Rathod, B., Hesketh, G.G., Abe, K.T., Youn, J.Y., Samavarchi-Tehrani, P., Zhang, H., Zhu, L.Y., et al. (2021). A proximity-dependent biotinylation map of a human cell. Nature *595*, 120–124. https://doi.org/10.1038/s41586-021-03592-2.
48. Yan, G., Yang, J., Li, W., Guo, A., Guan, J., and Liu, Y. (2023). Genome-wide CRISPR screens identify ILF3 as a mediator of mTORC1-dependent amino acid sensing. Nat. Cell Biol. *25*, 754–764. https://doi.org/10.1038/s41556-023-01123-x.
49. Thoreen, C.C., Chantranupong, L., Keys, H.R., Wang, T., Gray, N.S., and Sabatini, D.M. (2012). A unifying model for mTORC1-mediated regulation of mRNA translation. Nature *485*, 109–113. https://doi.org/10.1038/nature11083.
50. Dever, T.E., Dinman, J.D., and Green, R. (2018). Translation Elongation and Recoding in Eukaryotes. Cold Spring Harb. Perspect. Biol. *10*, a032649. https://doi.org/10.1101/cshperspect.a032649.
51. Meyuhas, O. (2008). Physiological roles of ribosomal protein S6: one of its kind. Int. Rev. Cell Mol. Biol. *268*, 1–37. https://doi.org/10.1016/S1937-6448(08)00801-0.
52. Ilik, I.A., Malszycki, M., Lubke, A.K., Schade, C., Meierhofer, D., and Aktas, T. (2020). SON and SRRM2 are essential for nuclear speckle formation. Elife *9*, e60579. https://doi.org/10.7554/eLife.60579.
53. Hsu, P.P., Kang, S.A., Rameseder, J., Zhang, Y., Ottina, K.A., Lim, D., Peterson, T.R., Choi, Y., Gray, N.S., Yaffe, M.B., et al. (2011). The mTOR-regulated phosphoproteome reveals a mechanism of mTORC1-mediated inhibition of growth factor signaling. Science *332*, 1317–1322. https://doi.org/10.1126/science.1199498.
54. Cuinat, S., Nizon, M., Isidor, B., Stegmann, A., van Jaarsveld, R.H., van Gassen, K.L., van der Smagt, J.J., Volker-Touw, C.M.L., Holwerda, S.J.B., Terhal, P.A., et al. (2022). Loss-of-function variants in SRRM2 cause a neurodevelopmental disorder. Genet. Med. *24*, 1774–1780. https://doi.org/10.1016/j.gim.2022.04.011.
55. Chartier-Harlin, M.C., Dachsel, J.C., Vilariño-Güell, C., Lincoln, S.J., Leprêtre, F., Hulihan, M.M., Kachergus, J., Milnerwood, A.J., Tapia, L., Song, M.S., et al. (2011). Translation initiator EIF4G1 mutations in familial Parkinson disease. Am. J. Hum. Genet. *89*, 398–406. https://doi.org/10.1016/j.ajhg.2011.08.009.
56. Hekman, K.E., Yu, G.Y., Brown, C.D., Zhu, H., Du, X., Gervin, K., Undlien, D.E., Peterson, A., Stevanin, G., Clark, H.B., et al. (2012). A conserved eEF2 coding variant in SCA26 leads to loss of translational fidelity and increased susceptibility to

proteostatic insult. Hum. Mol. Genet. *21*, 5472–5483. https://doi.org/10.1093/hmg/dds392.

57. Sun, Z., Amsterdam, A., Pazour, G.J., Cole, D.G., Miller, M.S., and Hopkins, N. (2004). A genetic screen in zebrafish identifies cilia genes as a principal cause of cystic kidney. Development *131*, 4085–4093. https://doi.org/10.1242/dev.01240.
58. Calhoun, J.D., Aziz, M.C., Happ, H.C., Gunti, J., Gleason, C., Mohamed, N., Zeng, K., Hiller, M., Bryant, E., Mithal, D.S., et al. (2022). mTORC1 functional assay reveals SZT2 loss-of-function variants and a founder in-frame deletion. Brain *145*, 1939–1948. https://doi.org/10.1093/brain/awab451.
59. Huttlin, E.L., Bruckner, R.J., Navarrete-Perea, J., Cannon, J.R., Baltier, K., Gebreab, F., Gygi, M.P., Thornock, A., Zarraga, G., Tam, S., et al. (2021). Dual proteome-scale networks reveal cell-specific remodeling of the human interactome. Cell *184*, 3022–3040.e28. https://doi.org/10.1016/j.cell.2021.04.011.
60. Saxton, R.A., and Sabatini, D.M. (2017). mTOR Signaling in Growth, Metabolism, and Disease. Cell *168*, 960–976. https://doi.org/10.1016/j.cell.2017.02.004.
61. Lai, Y., and Jiang, Y. (2020). Reciprocal Regulation between Primary Cilia and mTORC1. Genes *11*, 711. https://doi.org/10.3390/genes11060711.
62. Zhong, M., Zhao, X., Li, J., Yuan, W., Yan, G., Tong, M., Guo, S., Zhu, Y., Jiang, Y., Liu, Y., and Jiang, Y. (2016). Tumor Suppressor Folliculin Regulates mTORC1 through Primary Cilia. J. Biol. Chem. *291*, 11689–11697. https://doi.org/10.1074/jbc.M116.719997.
63. Takahashi, K., Nagai, T., Chiba, S., Nakayama, K., and Mizuno, K. (2018). Glucose deprivation induces primary cilium formation through mTORC1 inactivation. J. Cell Sci. *131*, jcs208769. https://doi.org/10.1242/jcs.208769.
64. Yuan, S., Li, J., Diener, D.R., Choma, M.A., Rosenbaum, J.L., and Sun, Z. (2012). Target-of-rapamycin complex 1 (Torc1) signaling modulates cilia size and function through protein synthesis regulation. Proc. Natl. Acad. Sci. USA *109*, 2021–2026. https://doi.org/10.1073/pnas.1112834109.
65. Nachury, M.V., Loktev, A.V., Zhang, Q., Westlake, C.J., Peränen, J., Merdes, A., Slusarski, D.C., Scheller, R.H., Bazan, J.F., Sheffield, V.C., and Jackson, P.K. (2007). A core complex of BBS proteins cooperates with the GTPase Rab8 to promote ciliary membrane biogenesis. Cell *129*, 1201–1213. https://doi.org/10.1016/j.cell.2007.03.053.
66. Casar Tena, T., Maerz, L.D., Szafranski, K., Groth, M., Blätte, T.J., Donow, C., Matysik, S., Walther, P., Jeggo, P.A., Burkhalter, M.D., and Philipp, M. (2019). Resting cells rely on the DNA helicase component MCM2 to build cilia. Nucleic Acids Res. *47*, 134–151. https://doi.org/10.1093/nar/gky945.
67. Devi, R., Pelletier, L., and Prosser, S.L. (2021). Charting the complex composite nature of centrosomes, primary cilia and centriolar satellites. Curr. Opin. Struct. Biol. *66*, 32–40. https://doi.org/10.1016/j.sbi.2020.10.006.
68. Ververi, A., Zagaglia, S., Menzies, L., Baptista, J., Caswell, R., Baulac, S., Ellard, S., Lynch, S., Jacques, T.S., et al.; Genomics England Research Consortium (2023). Germline homozygous missense DEPDC5 variants cause severe refractory early-onset epilepsy, macrocephaly and bilateral polymicrogyria. Hum. Mol. Genet. *32*, 580–594. https://doi.org/10.1093/hmg/ddac225.